Journal of Computational Physics 228 (2009) 3582–3604

Contents lists available at ScienceDirect

Journal of Computational Physics

journal homepage: www.elsevier.com/locate/jcp

Modified kinetic flux vector splitting schemes for compressible flows ☆

Yibing Chen *, Song Jiang

Institute of Applied Physics and Computational Mathematics, P.O. Box 8009, Beijing 100088, PR China

ARTICLE INFO

Article history:
Received 10 October 2007
Received in revised form 22 July 2008
Accepted 30 January 2009
Available online 14 February 2009

Keywords:
KFVS scheme
First- and second-order modified KFVS schemes
BGK scheme
Nonoscillatory
Contact discontinuities
Multi-fluids

ABSTRACT

We investigate the traditional kinetic flux vector splitting (KFVS) and BGK schemes for the compressible Euler equations. First, based on a careful study of the behavior of the discrete physical variables across the contact discontinuity, we analyze quantitatively the mechanism of inducing spurious oscillations of the velocity and pressure in the vicinity of the contact discontinuity for the first-order KFVS and BGK schemes. Then, with the help of this analysis, we propose a first-order modified KFVS (MKFVS) scheme which is oscillation-free in the vicinity of the contact discontinuity, provided certain consistent conditions are satisfied. Moreover, by using piecewise linear reconstruction and van Leer's limiter, the first-order MKFVS scheme is extended to a second-order one, consequently, a nonoscillatory second-order MKFVS scheme is constructed. Finally, by combing the MKFVS schemes with the γ-model, we successfully extend the MKFVS schemes to multi-flows, and propose therefore a first- and second-order MKFVS schemes for multi-fluid computations, which are nonoscillatory across fluid interfaces. A number of numerical examples presented in this paper validate the theoretic analysis and demonstrate the good performance of the MKFVS schemes in simulation of contact discontinuities for both single- and multi-fluids.

1. Introduction

In the past years the development of Boltzmann-type schemes for the simulation of compressible fluids has attracted much attention, and significant progress has been made in their construction and analysis. Also, the success of such schemes has appeared in a wide range of engineering applications, see for example, [5,6,10–14,16,17,19,21]. Among the Boltzmann-type schemes, the equilibrium-flux method (EFM) has been intensively studied [16]. EFM is flux splitting and is also referred to as a kinetic flux vector splitting (KFVS) scheme [16]. In fact, it is easy to see that the EFM and KFVS schemes are identical. The KFVS scheme is composed of two steps. Firstly, the free transport equation or the collisionless Boltzmann equation is solved in the gas evolution stage for the flux evaluation. Then, the collision part is implicitly implemented inside each cell through the preparation of a new equilibrium state inside each cell at the beginning of the next time step. Also, the KFVS scheme has been successfully applied to solving numerically various problems, see [3,4,8,9,14,16,17], for example. Two of the advantages of the KFVS scheme for the Euler equations are robust and Riemann-solver free, we do not need to find an exact or approximate Riemann solver. On the other hand, the KFVS scheme is based on the collisionless Boltzmann equation which could not capture the real gas dynamical property of the Euler equations (cf. [20, Chapters 3 and 4]). Although artificial collisions are added in the projection stage, spurious oscillations across the contact discontinuity have still been observed for the KFVS scheme, see the analysis in Section 2 and the numerical examples in Section 5.

☆ Supported by the Special Funds for Major State Basic Research Projects (Grant No. 2005CB321700), NSFC (Grant Nos. 10225105, 40890154 and 10802010), Science Foundation of CAEP (Grant No. 2007A09006).
* Corresponding author.
E-mail addresses: chen_yibing@iapcm.ac.cn (Y. Chen), jiang@iapcm.ac.cn (S. Jiang).

0021-9991/$ - see front matter © 2009 Elsevier Inc. All rights reserved.
doi:10.1016/j.jcp.2009.01.035

With the inclusion of the Boltzmann collision model in the flux evaluation process, the gas-kinetic BGK scheme has been proposed [15,22], which differs from the KFVS scheme mainly in the inclusion of particle collisions in the gas evolution stage. The BGK scheme makes use of the local integral solution of the collisional BGK model to compute a time-dependent gas distribution function at a cell interface and to obtain the numerical fluxes in the gas evolution stage. Since the BGK model is a statistical model, the particle transport and collision are coupled in the whole gas evolution process, and the particle collision time controls the physical dissipative coefficients in the macroscopic equations. Since the gas evolution is associated with a relaxation process, i.e., from a non-equilibrium state to an equilibrium one, the entropy condition is satisfied by the BGK scheme. Based on the Chapman–Enskog expansion, from the gas-kinetic BGK model the Euler as well as the Navier–Stokes equations can be derived. In the smooth flow region, as the flow structure can be well resolved by the numerical cell size, the BGK scheme goes back to the Lax–Wendroff-type method for the compressible Navier–Stokes equations. In the discontinuity region, a delicate dissipative mechanism due to both kinematic and dynamic dissipation in the BGK scheme presents a stable and crisp shock transition, see [13,21]. For the BGK schemes, however, as we will see from the analysis in Section 2 and the numerical examples in Section 5, spurious oscillations across the contact discontinuity can still be observed and will not vanish as the accuracy is improved. Such spurious oscillation phenomenon has been also observed and analyzed for certain Godunov-type schemes, see, for example, [1,2].

In this paper, we first analyze the mechanism of inducing oscillations for the first-order KFVS and BGK schemes and find the (consistent) conditions that enable the contact discontinuity to still remain a contact discontinuity. Then, based on this analysis, we propose a first-order modified KFVS (MKFVS) scheme that is oscillation-free across the contact discontinuity. Moreover, by using piecewise linear reconstruction and van Leer's limiter, the first-order MKFVS scheme is extended to a second-order one, and consequently, we obtain a nonoscillatory second-order MKFVS scheme. Finally, by combing the MKFVS schemes with the γ-model which tracks the motion of a fluid interface, we successfully extend the MKFVS schemes to multi-flows, and propose therefore a first- and second-order MKFVS schemes for multi-fluid computations, which are nonoscillatory across fluid interfaces. A number of one- and two-dimensional numerical tests are presented which validate the theoretic analysis and demonstrate the good performance of the MKFVS schemes in simulation of the contact discontinuity for both single- and multi-fluids.

The paper is organized as follows: In Section 2 we analyze numerical errors of the first-order KFVS and BGK schemes near contact discontinuities, and with the help of this analysis, we propose our first- and second-order nonoscillatory MKFVS schemes in Section 3. In Section 4, the MKFVS schemes of first- and second-order are successfully extend to multi-flows, resulting in a first- and second-order nonoscillatory MKFVS schemes for multi-fluid simulations. Finally, in Section 5 a number of one- and two-dimensional single- and multi-fluid numerical experiments are presented to compare three schemes: the KFVS, BGK and MKFVS schemes of first- and second-order. The numerical results validate the accuracy and non-oscillation of the MKFVS in computation of contact discontinuities for both single- and multi-fluids.

2. Error analysis for the KFVS and BGK schemes

In this section we will analyze numerical errors of the first-order KFVS and BGK schemes across the contact discontinuity. For simplicity, we assume that the velocity and pressure are uniform throughout the computational grid. The purpose in this section is to find conditions that enable the contact discontinuity to still remain a contact discontinuity. The basic idea in the analysis, inspired by the work of Abgrall [1], is to compare carefully the value of the conservative variables across the contact discontinuity at both nth and $(n+1)$th time steps, and try to find the quantity which induces oscillations. For the sake of clear presentation, we restrict our analysis to the one-dimensional case.

The one-dimensional compressible Euler equations, consisting of conservation of mass, momentum and energy, can be written in the following conservation form:

$$\frac{\partial \vec{W}}{\partial t}+\frac{\partial F(\vec{W})}{\partial x}=0, \tag{2.1}$$

where

$$\vec{W}=(\rho,\rho U,\rho E)^T,\quad F(\vec{W})=(\rho U,\rho U^2+P,\rho EU+PU)^T,\quad P=(\gamma-1)\rho e=(\gamma-1)\left(\rho E-\frac{1}{2}\rho U^2\right) \tag{2.2}$$

and ρ, U, E, P and γ denote the density, velocity, total energy, pressure, internal energy and the ratio of specific heats, respectively.

In order to quantitatively analyze spurious oscillations across the contact discontinuity, we consider the initial value problem for (2.1) and (2.2) with the following (specific) initial data, such that the solution of (2.1)–(2.3) consists of the contact discontinuity only

$$\vec{W}(x,0)=\begin{cases}(\rho_L,\rho_L U_L,\rho_L E_L), & x<0,\\ (\rho_R,\rho_R U_R,\rho_R E_R), & x>0,\end{cases} \tag{2.3}$$

where

$$\rho_L\neq\rho_R,\quad U_L=U_R,\quad P_L=P_R.$$

We call such problem the interface only problem for (2.1) and (2.2).

2.1. Error analysis for the first-order KFVS scheme

The first-order KFVS scheme for the Euler equations (2.1), (2.3) reads (cf. [16,20]):

$$\vec{W}_j^{n+1} = \vec{W}_j^n - \lambda\left[F_{j+1/2}^n - F_{j-1/2}^n\right], \tag{2.4}$$

where $\vec{W}_j^n$ is the cell averaged value of $\vec{W}$ in the cell j at time $n\Delta t$, $F_{j\pm1/2}^n$ are the numerical flux on the cell boundary at time $n\Delta t$ which can be decomposed into

$$F_{j+1/2}^n = F_j^{n,+} + F_{j+1}^{n,-}, \quad F_{j-1/2}^n = F_{j-1}^{n,+} + F_j^{n,-}$$

with

$$F_j^{n,\pm} = \langle u^1\rangle_{j,\pm}\begin{bmatrix}\rho\\ \rho U\\ \rho E\end{bmatrix}_j^n + \begin{bmatrix}0\\ P_j^n\langle u^0\rangle_{j,\pm}\\ \frac{1}{2}P_j^n\langle u^1\rangle_{j,\pm} + \frac{1}{2}P_j^nU_j^n\langle u^0\rangle_{j,\pm}\end{bmatrix}$$

and

$$\langle u^0\rangle_{j,\pm} = \frac{1}{2}\operatorname{erfc}\left(\mp\sqrt{\lambda_j^n}U_j^n\right),$$
$$\langle u^1\rangle_{j,\pm} = U_j^n\langle u^0\rangle_{j,\pm} \pm \frac{1}{2}\frac{e^{-\lambda_j^n(U_j^n)^2}}{\sqrt{\pi}\lambda_j^n},$$
$$\lambda_j^n = \frac{\rho_j^n}{2p_j^n},$$

In what follows in this section, we try to find the conditions that enable the contact discontinuity to still remain a contact discontinuity, i.e. $U_j^{n+1} = U_j^n$ and $P_j^{n+1} = P_j^n$ for any j under the conditions that $U_j^n = U_0$ and $P_j^n = P_0$, where P_0 and U_0 are constants.

We first consider the conservation law of mass. By virtue of (2.4), the density at $(n+1)$th time step can be expressed by the value of the density and velocity at nth time step in the following form:

$$\rho_j^{n+1} = \rho_j^n - \lambda((\rho U)_{j+1/2}^n - (\rho U)_{j-1/2}^n), \tag{2.5}$$

where

$$(\rho U)_{j+1/2}^n = (\rho U)_{j,+}^n + (\rho U)_{j+1,-}^n = \rho_j^n\langle u^1\rangle_{j,+} + \rho_{j+1}^n\langle u^1\rangle_{j+1,-},$$
$$(\rho U)_{j-1/2}^n = (\rho U)_{j-1,+}^n + (\rho U)_{j,-}^n = \rho_{j-1}^n\langle u^1\rangle_{j-1,+} + \rho_j^n\langle u^1\rangle_{j,-}.$$

Substituting the above identities into (2.5), we thus obtain

$$\rho_j^{n+1} = \rho_j^n - \lambda\left[\rho_{j+1}^n\langle u^1\rangle_{j+1,-} + \rho_j^n\langle u^1\rangle_{j,+} - \rho_j^n\langle u^1\rangle_{j,-} - \rho_{j-1}^n\langle u^1\rangle_{j-1,+}\right]. \tag{2.6}$$

To study the oscillation mechanism of the velocity and the pressure near the contact discontinuity, we assume that the density obtained by (2.6) are correct. Under this assumption, we then investigate the numerical errors of the velocity obtained by the conservation law of momentum. By virtue of (2.4), the momentum at time $(n+1)\Delta t$ can be expressed by the value of the momentum, density, velocity and pressure at time $n\Delta t$ in the following form:

$$(\rho U)_j^{n+1} = (\rho U)_j^n - \lambda\left((\rho U^2 + P)_{j+1/2}^n - (\rho U^2 + P)_{j-1/2}^n\right), \tag{2.7}$$

where

$$\begin{aligned}(\rho U^2 + P)_{j+1/2}^n &= (\rho U^2 + P)_{j,+}^n + (\rho U^2 + P)_{j+1,-}^n\\ &= \rho_j^nU_j^n\langle u^1\rangle_{j,+} + \rho_{j+1}^nU_{j+1}^n\langle u^1\rangle_{j+1,-} + P_j^n\langle u^0\rangle_{j,+} + P_{j+1}^n\langle u^0\rangle_{j+1,-},\\ (\rho U^2 + P)_{j-1/2}^n &= (\rho U^2 + P)_{j-1,+}^n + (\rho U^2 + P)_{j,-}^n\\ &= \rho_{j-1}^nU_{j-1}^n\langle u^1\rangle_{j-1,+} + \rho_j^nU_j^n\langle u^1\rangle_{j,-} + P_{j-1}^n\langle u^0\rangle_{j-1,+} + P_j^n\langle u^0\rangle_{j,-}.\end{aligned}$$

Hence, U_j^{n+1} is given by

$$\begin{aligned}U_j^{n+1} = \frac{1}{\rho_j^{n+1}}\Big\{&(\rho U)_j^n - \lambda\Big[\left(\rho_j^nU_j^n\langle u^1\rangle_{j,+} + \rho_{j+1}^nU_{j+1}^n\langle u^1\rangle_{j+1,-} + P_j^n\langle u^0\rangle_{j,+} + P_{j+1}^n\langle u^0\rangle_{j+1,-}\right)\\ &-\left(\rho_{j-1}^nU_{j-1}^n\langle u^1\rangle_{j-1,+} + \rho_j^nU_j^n\langle u^1\rangle_{j,-} + P_{j-1}^n\langle u^0\rangle_{j-1,+} + P_j^n\langle u^0\rangle_{j,-}\right)\Big]\end{aligned}$$

Since $U_j^n = U_0 = \text{const.}$, $P_j^n = P_0 = \text{const.}$ for all j, we have from the above identity that

$$U_j^{n+1} = \frac{U_0}{\rho_j^{n+1}}\left\{\rho_j^n - \lambda\left[\rho_j^n\langle u^1\rangle_{j,+} + \rho_{j+1}^n\langle u^1\rangle_{j+1,-} - \rho_{j-1}^n\langle u^1\rangle_{j-1,+} - \rho_j^n\langle u^1\rangle_{j,-}\right]\right\} - \frac{\lambda P_0}{\rho_j^{n+1}}\left\{\langle u^0\rangle_{j,+} + \langle u^0\rangle_{j+1,-} - \langle u^0\rangle_{j-1,+} - \langle u^0\rangle_{j,-}\right\}. \tag{2.8}$$

Substituting ρ_j^{n+1} from (2.6) into (2.8), we find that

$$U_j^{n+1} = U_0 - \varepsilon_0\lambda\frac{P_0}{\rho_j^{n+1}}, \tag{2.9}$$

where

$$\varepsilon_0 = \langle u^0\rangle_{j,+} + \langle u^0\rangle_{j+1,-} - \langle u^0\rangle_{j-1,+} - \langle u^0\rangle_{j,-}.$$

Next, we study the oscillatory phenomenon of the pressure. For this purpose, we assume that the computed velocity remains uniform across the contact discontinuity, i.e., $U_j^{n+1} = U_0$. Under this assumption, we then investigate numerical errors of the pressure in the vicinity of the contact discontinuity. Let us consider the conservation law of energy from which the discrete pressure is computed. By virtue of (2.4), the total energy at $(n+1)$th time step can be expressed by the value of the total energy, density, velocity and pressure at nth time step in the following form:

$$(\rho E)_j^{n+1} = (\rho E)_j^n - \lambda\left((\rho EU + PU)_{j+\frac{1}{2}}^n - (\rho EU + PU)_{j-\frac{1}{2}}^n\right), \tag{2.10}$$

where

$$(\rho EU + PU)_{j+1/2}^n = (\rho E)_j^n\langle u^1\rangle_{j,+} + \frac{1}{2}P_j^n\langle u^1\rangle_{j,+} + \frac{1}{2}P_j^nU_j^n\langle u^0\rangle_{j,+} + (\rho E)_{j+1}^n\langle u^1\rangle_{j+1,-} + \frac{1}{2}P_{j+1}^n\langle u^1\rangle_{j+1,-} + \frac{1}{2}P_{j+1}^nU_{j+1}^n\langle u^0\rangle_{j+1,-},$$
$$(\rho EU + PU)_{j-1/2}^n = (\rho E)_{j-1}^n\langle u^1\rangle_{j-1,+} + \frac{1}{2}P_{j-1}^n\langle u^1\rangle_{j-1,+} + \frac{1}{2}P_{j-1}^nU_{j-1}^n\langle u^0\rangle_{j-1,+} + (\rho E)_j^n\langle u^1\rangle_{j,-} + \frac{1}{2}P_j^n\langle u^1\rangle_{j,-} + \frac{1}{2}P_j^nU_j^n\langle u^0\rangle_{j,-}.$$

In view of (2.2), we may write

$$\rho E = \rho e + \frac{1}{2}\rho U^2 = \frac{P}{(\gamma-1)} + \frac{1}{2}\rho U^2. \tag{2.11}$$

Inserting the above relation into (2.10), we see that

$$\begin{aligned}(\rho E)_j^{n+1} &= \left(\frac{P}{\gamma-1} + \frac{1}{2}\rho U^2\right)_j^n - \lambda\left\{\left[\left(\frac{P}{\gamma-1} + \frac{1}{2}\rho U^2\right)_j^n\langle u^1\rangle_{j,+} + \frac{1}{2}P_j^n\langle u^1\rangle_{j,+} + \frac{1}{2}P_j^nU_j^n\langle u^0\rangle_{j,+}\right.\right.\\ &\quad\left.+\left(\frac{P}{\gamma-1} + \frac{1}{2}\rho U^2\right)_{j+1}^n\langle u^1\rangle_{j+1,-} + \frac{1}{2}P_{j+1}^n\langle u^1\rangle_{j+1,-} + \frac{1}{2}P_{j+1}^nU_{j+1}^n\langle u^0\rangle_{j+1,-}\right]\\ &\quad-\left[\left(\frac{P}{\gamma-1} + \frac{1}{2}\rho U^2\right)_{j-1}^n\langle u^1\rangle_{j-1,+} + \frac{1}{2}P_{j-1}^n\langle u^1\rangle_{j-1,+} + \frac{1}{2}P_{j-1}^nU_{j-1}^n\langle u^0\rangle_{j-1,+}\right.\\ &\quad\left.\left.+\left(\frac{P}{\gamma-1} + \frac{1}{2}\rho U^2\right)_j^n\langle u^1\rangle_{j,-} + \frac{1}{2}P_j^n\langle u^1\rangle_{j,-} + \frac{1}{2}P_j^nU_j^n\langle u^0\rangle_{j,-}\right]\right\}\\ &= \frac{1}{2}U_0^2\left[\rho_j^n - \lambda\left(\rho_{j+1}^n\langle u^1\rangle_{j+1,-} + \rho_j^n\langle u^1\rangle_{j,+} - \rho_j^n\langle u^1\rangle_{j,-} - \rho_{j-1}^n\langle u^1\rangle_{j-1,+}\right)\right]\\ &\quad+\frac{P_0}{\gamma-1} - \lambda\left(\frac{1}{\gamma-1} + \frac{1}{2}\right)P_0\left(\langle u^1\rangle_{j+1,-} + \langle u^1\rangle_{j,+} - \langle u^1\rangle_{j,-} - \langle u^1\rangle_{j-1,+}\right)\\ &\quad-\frac{\lambda}{2}P_0U_0\left(\langle u^0\rangle_{j+1,-} + \langle u^0\rangle_{j,+} - \langle u^0\rangle_{j,-} - \langle u^0\rangle_{j-1,+}\right)\\ &= \frac{1}{2}U_0^2\rho_j^{n+1} + \frac{P_0}{(\gamma-1)} - \lambda\frac{1}{2}P_0U_0\varepsilon_0 - \lambda\left(\frac{1}{\gamma-1} + \frac{1}{2}\right)P_0\varepsilon_1\end{aligned} \tag{2.12}$$

with

$$\varepsilon_1 = \langle u^1\rangle_{j+1,-} + \langle u^1\rangle_{j,+} - \langle u^1\rangle_{j,-} - \langle u^1\rangle_{j-1,+},$$
$$\varepsilon_0 = \langle u^0\rangle_{j+1,-} + \langle u^0\rangle_{j,+} - \langle u^0\rangle_{j,-} - \langle u^0\rangle_{j-1,+}.$$

By (2.12) and (2.11) from which P_j^{n+1} can be calculated, and (2.9) that gives U_j^{n+1}, we find that if the following conditions hold:

$$\varepsilon_0 = 0, \quad \varepsilon_1 = 0, \tag{2.13}$$

then, across the contact discontinuity, the pressure and velocity satisfy

$$P_j^{n+1} = P_j^n = P_0, \quad U_j^{n+1} = U_j^n = U_0.$$

That means that if (2.13) is satisfied, then there will be no spurious oscillations present in the pressure and velocity in the vicinity of the contact discontinuity.

2.2. Error analysis for the first-order BGK scheme

In this section, we will analyze the numerical error of the BGK scheme across the contact discontinuity. According to [15,20,22], the first-order BGK scheme can be written as

$$\vec{W}_j^{n+1} = \vec{W}_j^n - \lambda\left[F_{j+1/2}^{n,B} - F_{j-1/2}^{n,B}\right], \tag{2.14}$$

where

$$F_{j+1/2}^{n,B} = F_j^{n,B,+} + F_{j+1}^{n,B,-}, \quad F_{j-1/2}^{n,B} = F_{j-1}^{n,B,+} + F_j^{n,B,-}.$$

It is also pointed out in [15,20,22] that the flux $F_{j+1/2}^{n,B}$ of the BGK scheme can be decomposed into

$$F_{j+1/2}^{n,B} = (1-\eta)F_{j+1/2}^{n,K} + \eta F_{j+1/2}^{n,E} \tag{2.15}$$

with $F_{j+1/2}^{n,K}$ being the flux of the KFVS scheme and $F_{j+1/2}^{n,E}$ the equilibrium state which is constructed by the conservation quantities on the both sides of a cell interface. More precisely, $F_{j+1/2}^{n,E}$ has the following form:

$$\begin{bmatrix}\rho\\ \rho U\\ \rho E\end{bmatrix}_{j+1/2}^{n,E} = \begin{bmatrix}\rho_j^{n,K}\langle u^0\rangle_{j,+} + \rho_{j+1}^{n,K}\langle u^0\rangle_{j+1,-}\\ \rho_j^{n,K}\langle u^1\rangle_{j,+} + \rho_{j+1}^{n,K}\langle u^1\rangle_{j+1,-}\\ \frac{1}{2}\rho_j^{n,K}U_j^{n,K}\langle u^1\rangle_{j,+} + \frac{1}{2}\rho_{j+1}^{n,K}U_{j+1}^{n,K}\langle u^1\rangle_{j+1,-} + \rho_j^{n,K}e_j^{n,K}\langle u^0\rangle_{j,+} + \rho_{j+1}^{n,K}e_{j+1}^{n,K}\langle u^0\rangle_{j+1,-}\end{bmatrix}.$$

Next, we analyze numerical errors (oscillations) across the contact discontinuity by checking whether the scheme (2.14) satisfies the (oscillation-free) conditions (2.20), (2.21). To this end, we easily deduce by a straightforward calculation that across the cell interface on which the contact discontinuity is located,

$$\begin{aligned}(\rho U)_{j+1/2}^{n,E} &= \rho_j^{n,K}\langle u^1\rangle_{j,+} + \rho_{j+1}^{n,K}\langle u^1\rangle_{j+1,-} = \rho_j^{n,K}\left(U_j^{n,K}\langle u^0\rangle_{j,+} + \frac{1}{2}\frac{e^{-\lambda_j^{n,K}(U_j^{n,K})^2}}{\sqrt{\pi\lambda_j^{n,K}}}\right) + \rho_{j+1}^{n,K}\left(U_{j+1}^{n,K}\langle u^0\rangle_{j+1,-} - \frac{1}{2}\frac{e^{-\lambda_{j+1}^{n,K}(U_{j+1}^{n,K})^2}}{\sqrt{\pi\lambda_{j+1}^{n,K}}}\right)\\ &:= \rho_{j+1/2}^{n,E}U_0 + \rho_j^{n,K}\varepsilon_j - \rho_{j+1}^{n,K}\varepsilon_{j+1},\end{aligned} \tag{2.16}$$

where

$$\varepsilon_j = \frac{1}{2}\frac{e^{-\lambda_j^{n,K}(U_j^{n,K})^2}}{\sqrt{\pi\lambda_j^{n,K}}}$$

and

$$\begin{aligned}(\rho E)_{j+1/2}^{n,E} &= \frac{1}{2}\rho_j^{n,K}U_j^{n,K}\langle u^1\rangle_{j,+} + \frac{1}{2}\rho_{j+1}^{n,K}U_{j+1}^{n,K}\langle u^1\rangle_{j+1,-} + \rho_j^{n,K}e_j^{n,K}\langle u^0\rangle_{j,+} + \rho_{j+1}^{n,K}e_{j+1}^{n,K}\langle u^0\rangle_{j+1,-}\\ &= \frac{1}{2}U_0(\rho U)_{j+1/2}^{n,E} + \frac{P_0}{\gamma-1}(\langle u^0\rangle_{j,+} + \langle u^0\rangle_{j+1,-}).\end{aligned} \tag{2.17}$$

From (2.16) and (2.17), we easily get

$$U_{j+1/2}^{n,E} = U_0 + \frac{\rho_j^{n,K}\varepsilon_{j,+} - \rho_{j+1}^{n,K}\varepsilon_{j+1,-}}{\rho_{j+1/2}^{n,E}}$$

and

$$\begin{aligned}P_{j+1/2}^{n,E} &= (\gamma-1)\left(\rho E - \frac{1}{2}\rho U^2\right)_{j+1/2}^{n,E} = P_0(\langle u^0\rangle_{j,+} + \langle u^0\rangle_{j+1,-}) + (\gamma-1)\left(\frac{1}{2}U_0(\rho U)_{j+1/2}^{n,E} - \frac{1}{2}U_{j+1/2}^{n,E}(\rho U)_{j+1/2}^{n,E}\right)\\ &= P_0(\langle u^0\rangle_{j,+} + \langle u^0\rangle_{j+1,-}) + \frac{1}{2}(\gamma-1)(\rho U)_{j+1/2}^{n,E}(U_0 - U_{j+1/2}^{n,E}).\end{aligned}$$

Therefore, we have

$$(PU)_{j+1/2}^{n,E} = P_0U_0(\langle u^0\rangle_{j,+} + \langle u^0\rangle_{j+1,-}) + U_0\frac{1}{2}(\gamma-1)(\rho U)_{j+1/2}^{n,E}(U_0 - U_{j+1/2}^{n,E}) + P_{j+1/2}^{n,E}\frac{(\rho_j^{n,K}\varepsilon_j - \rho_{j+1}^{n,K}\varepsilon_{j+1})}{\rho_{j+1/2}^{n,E}}.$$

By combing $P^{n,K}_{j+1/2}, P^{n,E}_{j+1/2}, (PU)^{n,K}_{j+1/2}$ and $(PU)^{n,E}_{j+1/2}$, we obtain immediately

$$P^{n,B}_{j+1/2} = (1-\eta)P^{n,K}_{j+1/2} + \eta P^{n,E}_{j+1/2} = P_0 + P_0(\langle u^0\rangle_{j,+} + \langle u^0\rangle_{j+1,-} - 1) + \eta\frac{1}{2}(\gamma-1)(\rho U)^{n,E}_{j+1/2}(U_0 - U^{n,E}_{j+1/2}) \tag{2.18}$$

and because

$$\begin{aligned}(PU)^{n,K}_{j+\frac{1}{2}} &= \frac{1}{2}[P^{n,K}_j\langle u^1\rangle_{j,+} + P^{n,K}_{j+1}\langle u^1\rangle_{j+1,-} + P^{n,K}_j U^{n,K}_j\langle u^0\rangle_{j,+} + P^{n,K}_{j+1}U^{n,K}_{j+1}\langle u^0\rangle_{j+1,-}]\\ &= \frac{1}{2}P_0(\langle u^1\rangle_{j,+} + \langle u^1\rangle_{j+1,-}) + \frac{1}{2}P_0U_0(\langle u^0\rangle_{j,+} + \langle u^0\rangle_{j+1,-})\\ &= \frac{1}{2}P_0(U_0\langle u^0\rangle_{j,+} + \varepsilon_j + U_0\langle u^0\rangle_{j+1,-} - \varepsilon_{j+1}) + \frac{1}{2}P_0U_0(\langle u^0\rangle_{j,+} + \langle u^0\rangle_{j+1,-}) = P_0U_0(\langle u^0\rangle_{j,+} + \langle u^0\rangle_{j+1,-}) + \frac{1}{2}P_0(\varepsilon_j - \varepsilon_{j+1})\end{aligned}$$

we have

$$\begin{aligned}(PU)^{n,B}_{j+1/2} &= (1-\eta)(PU)^{n,K}_{j+1/2} + \eta(PU)^{n,E}_{j+1/2}\\ &= P_0U_0(\langle u^0\rangle_{j,+} + \langle u^0\rangle_{j+1,-}) + \frac{(1-\eta)}{2}P_0(\varepsilon_j - \varepsilon_{j+1}) + \eta\left(U_0\frac{1}{2}(\gamma-1)(\rho U)^{n,E}_{j+1/2}(U_0 - U^{n,E}_{j+1/2}) + P^{n,E}_{j+\frac{1}{2}}\frac{\rho^{n,K}_j\varepsilon_j - \rho^{n,K}_{j+1}\varepsilon_{j+1}}{\rho^{n,E}_{j+1/2}}\right).\end{aligned} \tag{2.19}$$

Thus, by virtue of (2.18) and (2.19), $P^{n+1}_j = P_0$ and $U^{n+1}_j = U_0$ for any j if the following conditions are satisfied:

$$P_0(\langle u^0\rangle_{j,+} + \langle u^0\rangle_{j+1,-} - 1) + \eta\frac{1}{2}(\gamma-1)(\rho U)^{n,E}_{j+\frac{1}{2}}(U_0 - U^{n,E}_{j+\frac{1}{2}}) = 0, \tag{2.20}$$

$$P_0U_0(\langle u^0\rangle_{j,+} + \langle u^0\rangle_{j+1,-} - 1) + \frac{(1-\eta)}{2}P_0(\varepsilon_j - \varepsilon_{j+1}) + \eta\left(U_0\frac{1}{2}(\gamma-1)(\rho U)^{n,E}_{j+1/2}(U_0 - U^{n,E}_{j+1/2}) + P^{n,E}_{j+1/2}\frac{\rho^{n,K}_j\varepsilon_j - \rho^{n,K}_{j+1}\varepsilon_{j+1}}{\rho^{n,E}_{j+1/2}}\right) = 0. \tag{2.21}$$

From (2.20) and (2.21), we easily see that it is difficult to choose a suitable η satisfying simultaneously the above two equations. That means that certain oscillation across the contact discontinuity, although very small in amplitude, would be present in the first-order BGK scheme and could persist with refinement of meshes. On the other hand, our numerical examples show that the numerical errors of the BGK scheme near the contact discontinuity are smaller than those of the KFVS scheme. From the view point of kinetic theory, it is known that the real state of the contact discontinuity should lie between the collisionless and the equilibrium states. Consequently, η should be in $[0, 1]$. However, the choice of η is problem- and the user's experience-dependent.

3. Modified KFVS schemes

According to the analysis in Section 2, we see that across the contact discontinuity, if $U_L = U_R = U_0, P_L = P_R = P_0$ at $t = t^n$, then the conditions (2.13) guarantee no oscillation at $t = t^{n+1}$. There may be many choices to make (2.13) hold, and next we give the conditions (i.e. (3.2)) that imply (2.13) and more reasonable.

In fact, if across the contact discontinuity, $P^n_j = P^n_{j+1} = P_0$ and $U^n_j = U^n_{j+1} = U_0$, then the following fluxes across the contact discontinuity have to satisfy the following equations:

$$P^n_{j+1/2} = P_0, \quad P^n_{j+1/2}U^n_{j+\frac{1}{2}} = P_0U_0. \tag{3.1}$$

We call (3.1) the *consistent conditions*. Then, we have under (3.1) that

$$\begin{aligned}&P^n_{j+1/2} = P^n_j\langle u^0\rangle_{j,+} + P^n_{j+1}\langle u^0\rangle_{j+1,-} = P_0,\\ &P^n_{j+1/2}U^n_{j+1/2} = P^n_j\langle u^1\rangle_{j,+} + P^n_{j+1}\langle u^1\rangle_{j+1,-} = P_0U_0,\end{aligned}$$

from which it follows that

$$\begin{aligned}&\langle u^0\rangle_{j,+} + \langle u^0\rangle_{j+1,-} = 1,\\ &\langle u^1\rangle_{j,+} + \langle u^1\rangle_{j+1,-} = U_0.\end{aligned} \tag{3.2}$$

It is easy to see that the conditions (2.13) may not imply (3.1) in the vicinity of the contact discontinuity, while (3.2) do guarantee (3.1). Therefore, the conditions (3.2) are in general more reasonable than (2.13). Thus, we will modify the KFVS scheme using (3.2).

As aforementioned, if the consistent conditions hold, then the spurious oscillation (numerical error) will vanish. In view of the above analysis and in order to diminish oscillations across the contact discontinuity, we modify the first-order KFVS

scheme by replacing $\langle u^{0,1}\rangle_{j,\pm}$ in the fluxes in (2.4) by appropriate values to propose a new KFVS scheme of first order without oscillations across the contact discontinuity, which is described in the following.

The value of the conservative variables at $(n+1)$th time step is given by

$$\vec{W}_j^{n+1} = \vec{W}_j^n - \lambda[F_{j+1/2}^n - F_{j-1/2}^n], \tag{3.3}$$

where

$$F_{j+\frac{1}{2}}^n = F_j^{n,+} + F_{j+1}^{n,-}, \quad F_{j-\frac{1}{2}}^n = F_{j-1}^{n,+} + F_j^{n,-}$$

and

$$F_j^{n,\pm} = \langle u^1\rangle_{j,\pm}^* \begin{bmatrix} \rho \\ \rho U \\ \rho E \end{bmatrix}_j^n + \begin{bmatrix} 0 \\ P_j^n \langle u^0\rangle_{j,\pm}^* \\ \frac{1}{2} P_j^n \langle u^1\rangle_{j,\pm}^* + \frac{1}{2} P_j^n U_j^n \langle u^0\rangle_{j,\pm}^* \end{bmatrix}$$

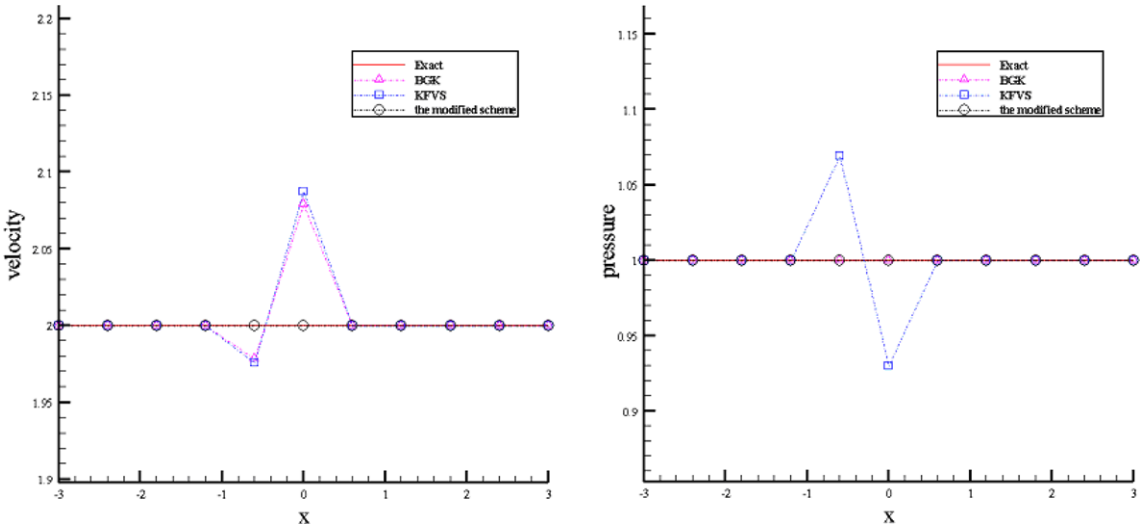

Fig. 1(a). Example 5.1: Computed results at $t = 0.3$ by the first-order BGK, KFVS and MKFVS schemes with 10 uniform cells. Left: the velocity; Right: the pressure.

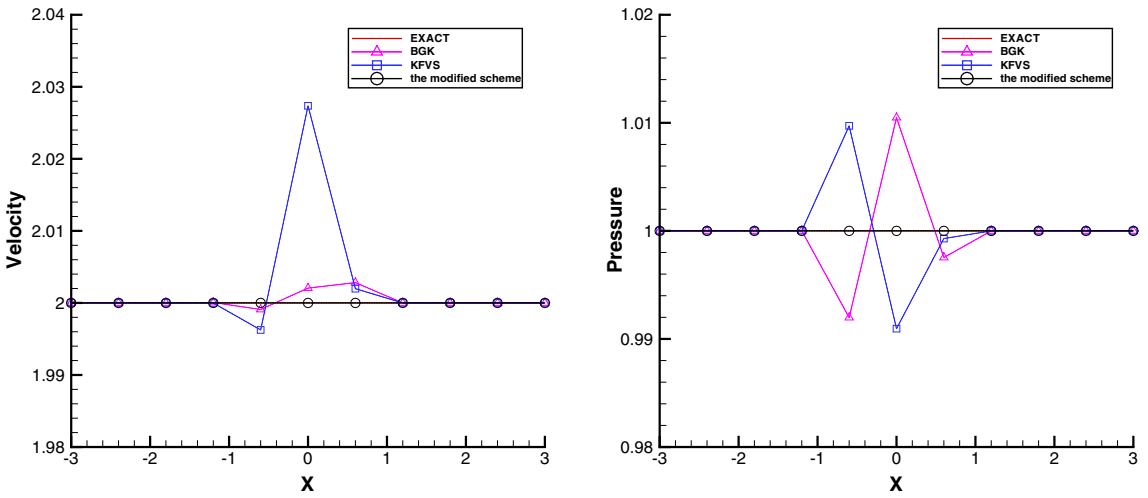

Fig. 1(b). Example 5.1: Computed results at $t = 0.3$ by the second-order BGK, KFVS and MKFVS schemes with 10 uniform cells. Left: the velocity; Right: the pressure.

with

$$\langle u^0\rangle^*_{j,\pm} = \frac{1}{2}\operatorname{erfc}\left(\mp\sqrt{\lambda^{n,*}_{j,\pm}}U^n_j\right), \quad \langle u^1\rangle^*_{j,\pm} = U^n_j\langle u^0\rangle^*_{j,\pm} \pm \frac{1}{2}\frac{e^{-\lambda^{n,*}_{j,\pm}(U^n_j)^2}}{\sqrt{\pi}\lambda^{n,*}_{j,\pm}}, \tag{3.4}$$

where

$$\lambda^{n,*}_{j,+} = \frac{\rho^n_j + \rho^n_{j+1}}{4P^n_j}, \quad \lambda^{n,*}_{j,-} = \frac{\rho^n_j + \rho^n_{j-1}}{4P^n_j}. \tag{3.5}$$

Inserting (3.5) into (3.4), we easily see that for our modified scheme, the conditions (3.2) hold. Hence, the consistent conditions (3.1) are satisfied for the modified scheme. We call the above scheme the modified KFVS scheme (MKFVS) of first order.

Remark 3.1. In the derivation of the first-order MKFVS scheme, in order to satisfy the consistent conditions (3.1), it suffices to make $\lambda^{n,*}_{j,+} = \lambda^{n,*}_{j+1,-}$, from which we deduce the formula (3.5).

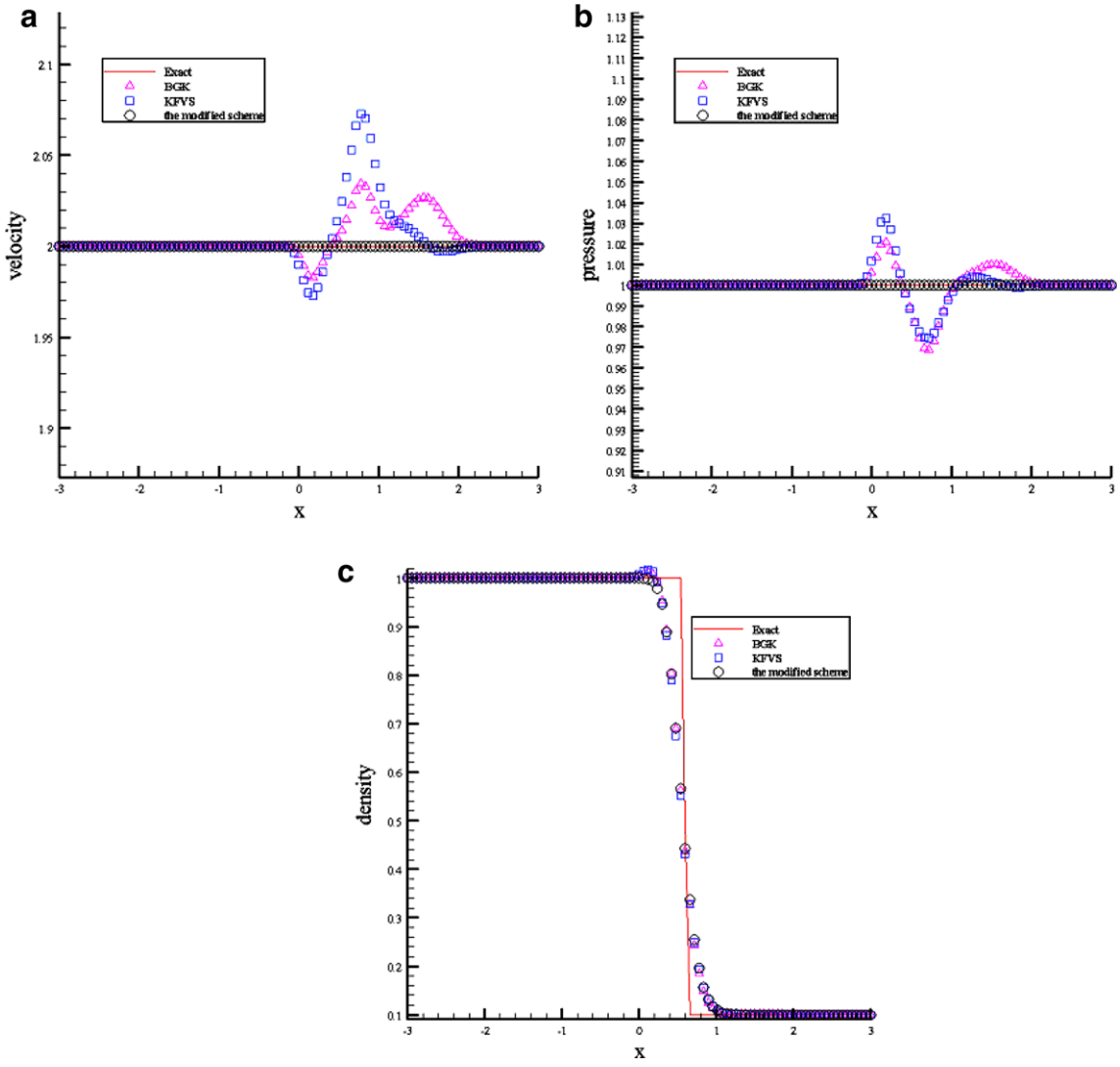

Fig. 2(a). Example 5.1: Computed results at $t = 0.3$ by the three first-order schemes with 100 uniform cells. (a) Velocity; (b) Pressure; (c) Density.

It is straightforward to extend our first-order scheme to a second-order one. Here we show how to construct a second-order MKFVS scheme. In the case of first-order accuracy, the distribution of the physical quantities is piecewise-constant within each cell. To reach second-order accuracy, instead of the constant distribution, we only need to reconstruct piecewise linear distribution of the physical quantities within each cell:

$$W_j^{(k)}(x) = W_j^{(k)} + \frac{\partial W^{(k)}}{\partial x}\left(x - x_{j+\frac{1}{2}}\right), \quad x \in (x_j, x_{j+1}), \tag{3.6}$$

where $W_j^{(k)}$ is the kth component of $\vec{W}_j$.

To avoid spurious oscillations across strong discontinuities, we employ van Leer's limiter to construct the slope:

$$L(s,r) = (\mathrm{sign}(s) + \mathrm{sign}(r))\frac{sr}{|s| + |r|},$$

where

$$s = \frac{W_{j+1}^{(k)} - W_j^{(k)}}{x_{j+1} - x_j}, \quad r = \frac{W_j^{(k)} - W_{j-1}^{(k)}}{x_j - x_{j-1}}.$$

Then, the reconstructed linear distribution of the physical quantities in the cell j is taken to be

$$W_j^{(k)}(x) = W_j^{(k)} + L(s,r)(x - x_{j+1/2}), \quad x \in (x_j, x_{j+1})$$

and the new physical quantities at two boundary nodes of the cell j are given by

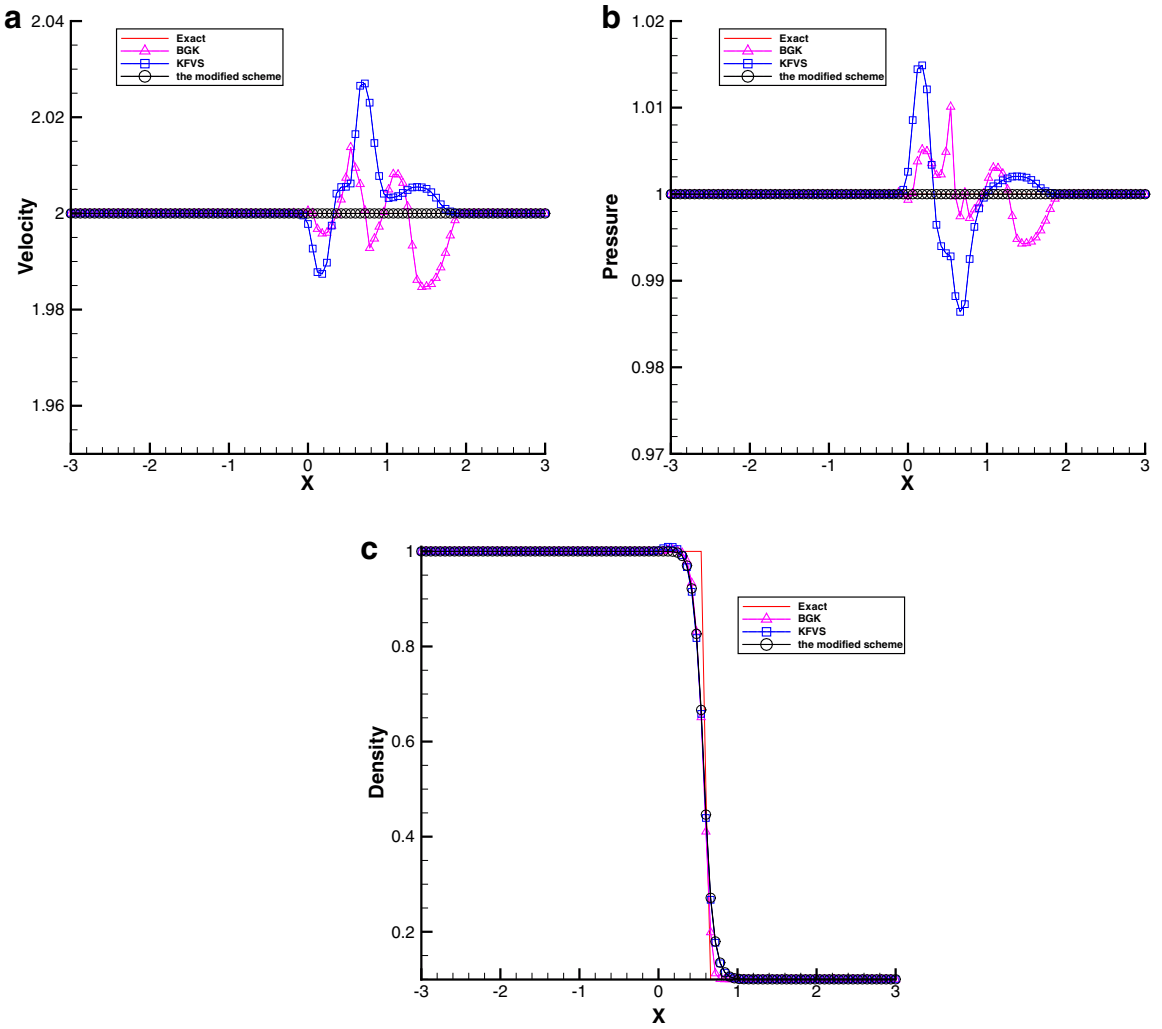

Fig. 2(b). Example 5.1: Computed results at $t = 0.3$ by the three second-order schemes with 100 uniform cells. (a) Velocity; (b) Pressure; (c) Density.

$$W_{j,+}^{(k)} = W_j^{(k)} + L(s,r)\cdot(x_{j+1} - x_{j+1/2}), \quad W_{j,-}^{(k)} = W_j^{(k)} - L(s,r)\cdot(x_{j+1/2} - x_j),$$

where $W_{j,+}^{(k)}$ and $W_{j,-}^{(k)}$ represent the value of the physical quantities at the right and left boundary nodes of the cell j, respectively.

Using this piecewise linear reconstruction, we can construct the numerical fluxes at a cell interface in the same manner as for the first-order scheme. Hence, our modified second-order (oscillation-free) KFVS scheme is written as follows:

$$\vec{W}_j^{n+1} = \vec{W}_j^n - \lambda\left[F_{j+1/2}^n - F_{j-1/2}^n\right] \tag{3.7}$$

with

$$F_{j+\frac{1}{2}}^n = F_j^{n,+} + F_{j+1}^{n,-}, \quad F_{j-\frac{1}{2}}^n = F_{j-1}^{n,+} + F_j^{n,-}$$

and

$$F_j^{n,\pm} = \langle u^1\rangle_{j,\pm}^* \begin{bmatrix}\rho\\ \rho U\\ \rho E\end{bmatrix}_{j,\pm}^n + \begin{bmatrix}0\\ P_{j,\pm}^n\langle u^0\rangle_{j,\pm}^*\\ \frac{1}{2}P_{j,\pm}^n\langle u^1\rangle_{j,\pm}^* + \frac{1}{2}P_{j,\pm}^n U_{j,\pm}^n\langle u^0\rangle_{j,\pm}^*\end{bmatrix},$$

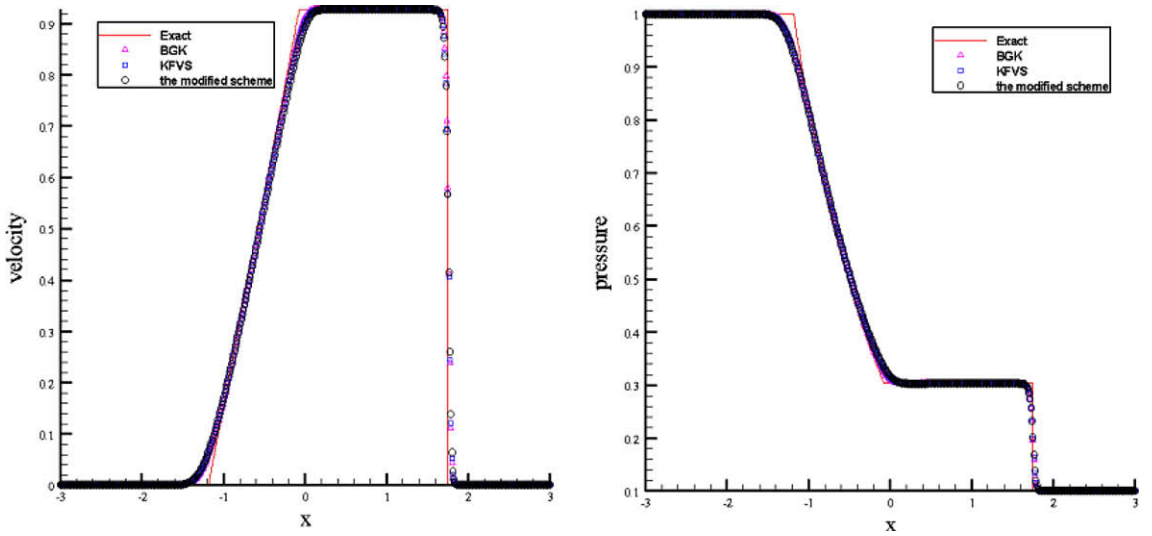

Fig. 3(a). Example 5.2: Computed results at $t = 1.0$ by the first-order BGK, FKVS and MFKVS schemes with 500 uniform cells. Left: Velocity; Right: Pressure.

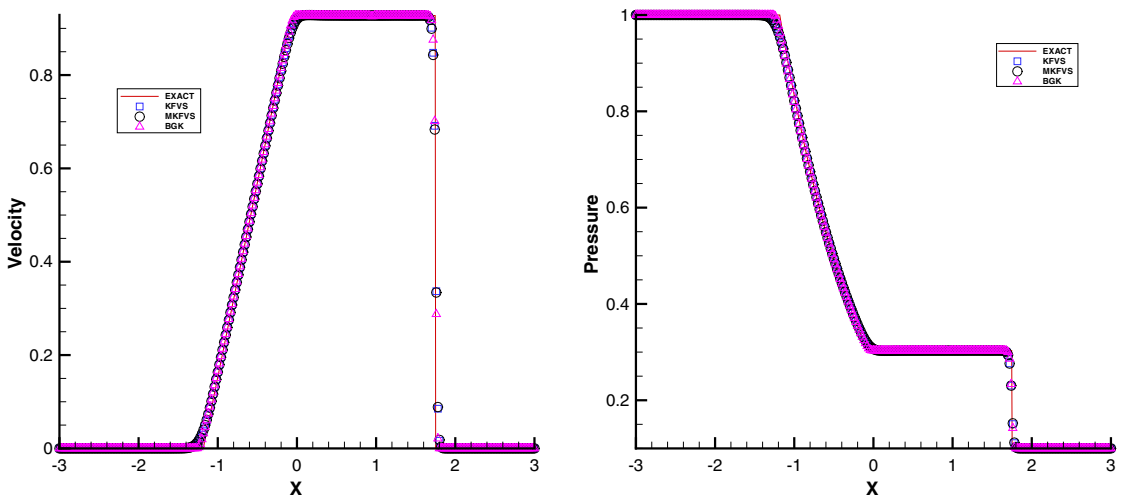

Fig. 3(b). Example 5.2: Computed results at $t = 1.0$ by the second-order BGK, FKVS and MFKVS schemes with 300 uniform cells. Left: Velocity; Right: Pressure.

where

$$\langle u^0\rangle^*_{j,\pm} = \frac{1}{2}\,\mathrm{erfc}\left(\mp\sqrt{\lambda^{n,*}_{j,\pm}}U^n_{j,\pm}\right), \quad \langle u^1\rangle^*_{j,\pm} = U^n_{j,\pm}\langle u^0\rangle^*_{j,\pm} \pm \frac{1}{2}\frac{e^{-\lambda^{n,*}_{j,\pm}(U^n_{j,\pm})^2 n,*}}{\sqrt{\pi}\lambda_{j,\pm}}$$

and

$$\lambda^{n,*}_{j,+} = \frac{1}{2}(\rho^n_{j,+} + \rho^n_{j+1,-})/2/p^n_{j,+}, \quad \lambda^{n,*}_{j,-} = \frac{1}{2}(\rho^n_{j,-} + \rho^n_{j-1,+})/2/p^n_{j,-}.$$

Instead of the forward difference in time in (3.7), we may use the second-order Runge–Kutta algorithm in the time discretization and obtain the following scheme which is of second-order accuracy both in time and in space:

$$\begin{aligned}\vec{W}^*_j &= \vec{W}^n_j - \lambda\left[F_{j+1/2}(\vec{W}^n) - F_{j-1/2}(\vec{W}^n)\right],\\ \vec{W}^{n+1}_j &= \frac{1}{2}(\vec{W}^n_j + \vec{W}^*_j) - \frac{1}{2}\lambda\left[F_{j+1/2}(\vec{W}^*) - F_{j-1/2}(\vec{W}^*)\right].\end{aligned} \tag{3.8}$$

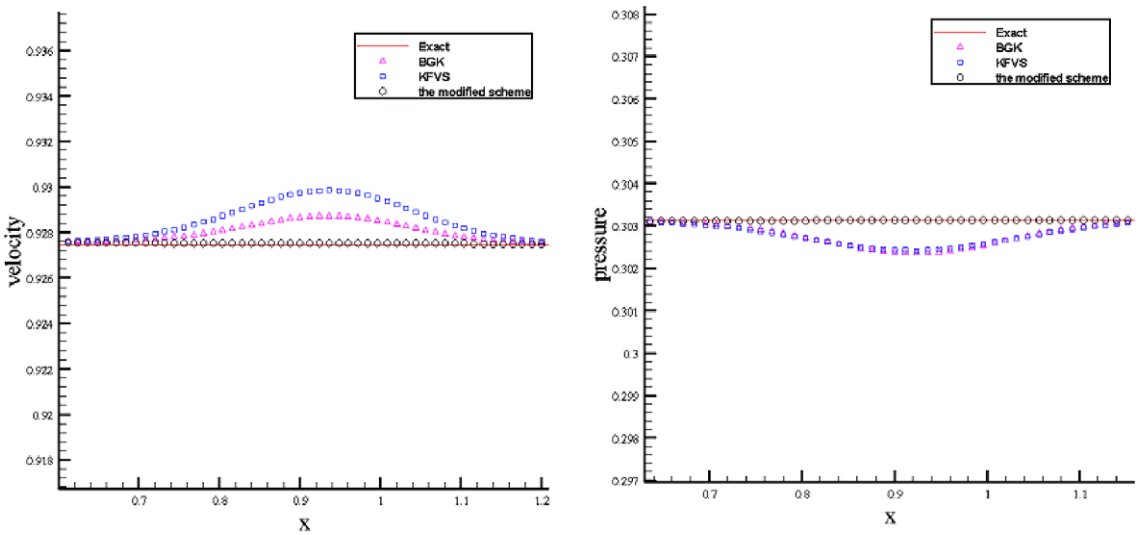

Fig. 4(a). Example 5.2: Close-up of the velocity and the pressure in the vicinity of the contact discontinuity in Fig. 3(a). Left: Velocity; Right: Pressure.

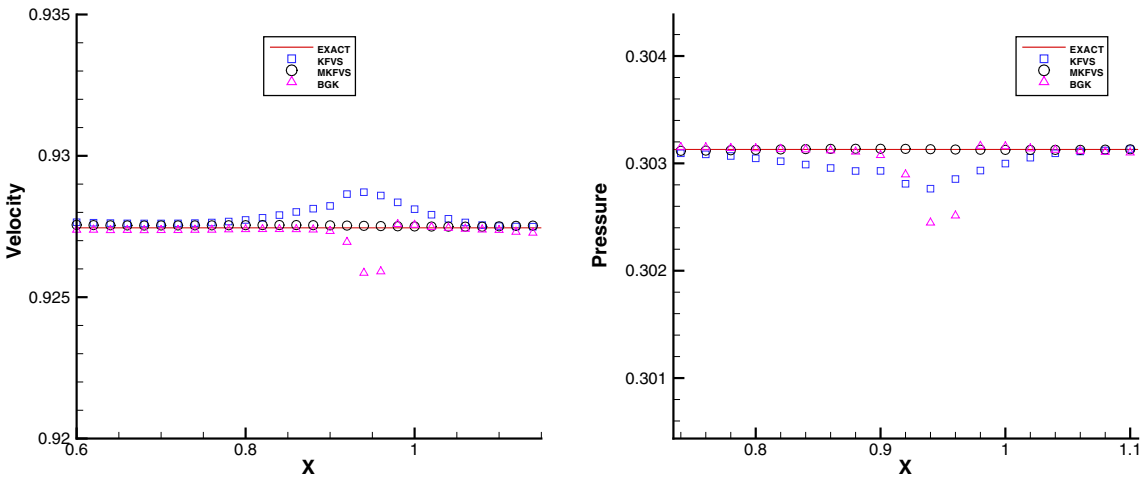

Fig. 4(b). Example 5.2: Close-up of the velocity and the pressure in the vicinity of the contact discontinuity in Fig. 3(b). Left: Velocity; Right: Pressure.

4. Extension to multi-fluids

Following Abgrall's work [1,2], we extend our first- and second-order MKFVS schemes constructed in the last section to multi-fluids. Consider the Euler equations (2.1), (2.2) for two fluids with different ratios of specific heats γ. Then, the fluid interface is described by the contact discontinuity of γ, and the motion of the fluid interface is governed by

$$\gamma_t + U\gamma_x = 0. \tag{4.1}$$

As analyzed in [1,2], to diminish possible spurious oscillations across the fluid interface, instead of (4.1), we should use the equation

$$\left[\frac{1}{\gamma-1}\right]_t + U\left[\frac{1}{\gamma-1}\right]_x = 0 \tag{4.2}$$

to capture the fluid interface.

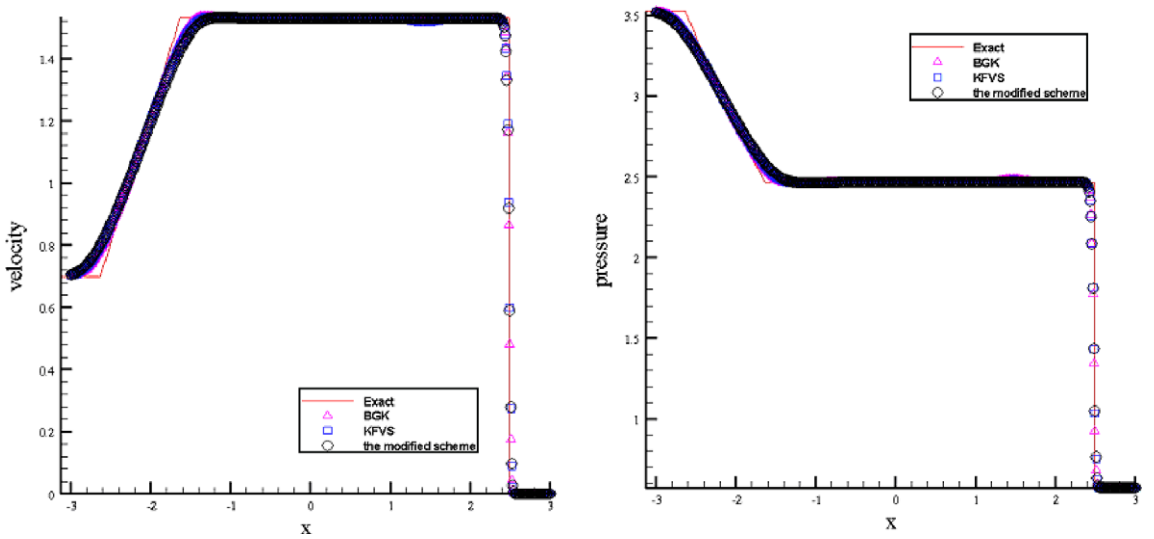

Fig. 5(a). Example 5.3: Computed results at $t = 1.0$ by the first-order BGK, KFVS and MKFVS schemes with 500 uniform cells. Left: Velocity; Right: Pressure.

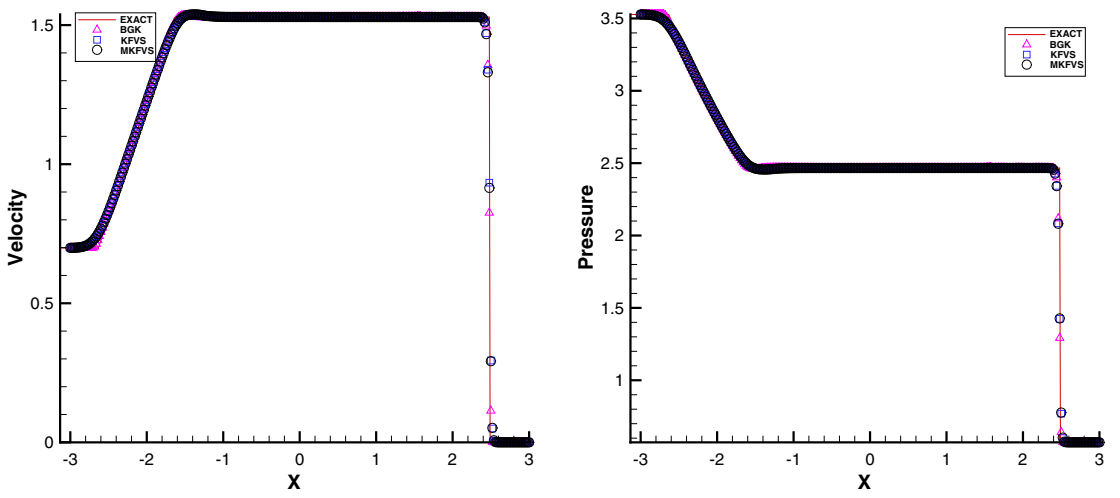

Fig. 5(b). Example 5.3: Computed results at $t = 1.0$ by the second-order BGK, KFVS and MKFVS schemes with 500 uniform cells. Left: Velocity; Right: Pressure.

By numerically solving the coupled equations (2.1), (2.2) and (4.2), we can find the location of the fluid interface as the discontinuity of γ at any time. In this section, we apply the first- and second-order MKFVS schemes to the coupled system (2.1), (2.2) and (4.2), and propose therefore the first- and second-order MKFVS schemes for multi-fluid computations.

To analyze possible oscillations across the fluid interface, we consider the interface only problem for (2.1), (2.2) and (4.2) with initial data

$$\vec{W}(x,0) = \begin{cases} (\rho_L, \rho_L U_L, \rho_L E_L, \gamma_L), & x < 0, \\ (\rho_R, \rho_R U_R, \rho_R E_R, \gamma_R), & x > 0, \end{cases} \tag{4.3}$$

where

$$\rho_L \neq \rho_R, \quad \gamma_L \neq \gamma_R, \quad U_L = U_R = U_0 = \text{const.}, \quad P_L = P_R = P_0 = \text{const.}.$$

We apply the first-order MKFVS scheme to solve (2.1), (2.2), (4.2) and (4.3), and obtain the first-order MKFVS scheme for multi-fluids. To analyze possible oscillations for this scheme, we deduce in the same manner as for the KFVS scheme in Section 2 to obtain, after omitting the superscript of $*$ for simplicity, that

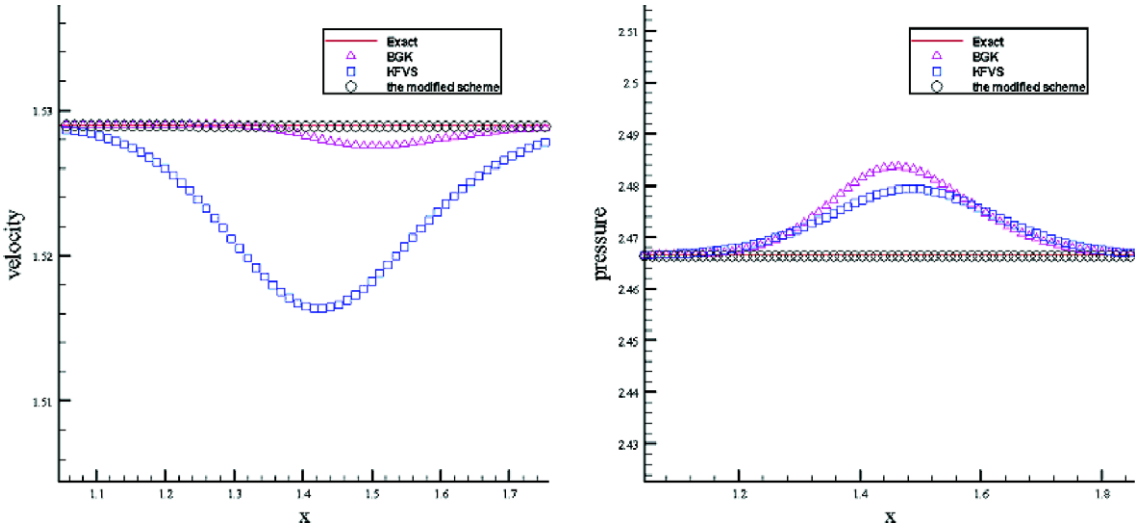

Fig. 6(a). Example 5.3: Close-up in the vicinity of the contact discontinuity in Fig. 5(a). Left: Velocity; Right: Pressure.

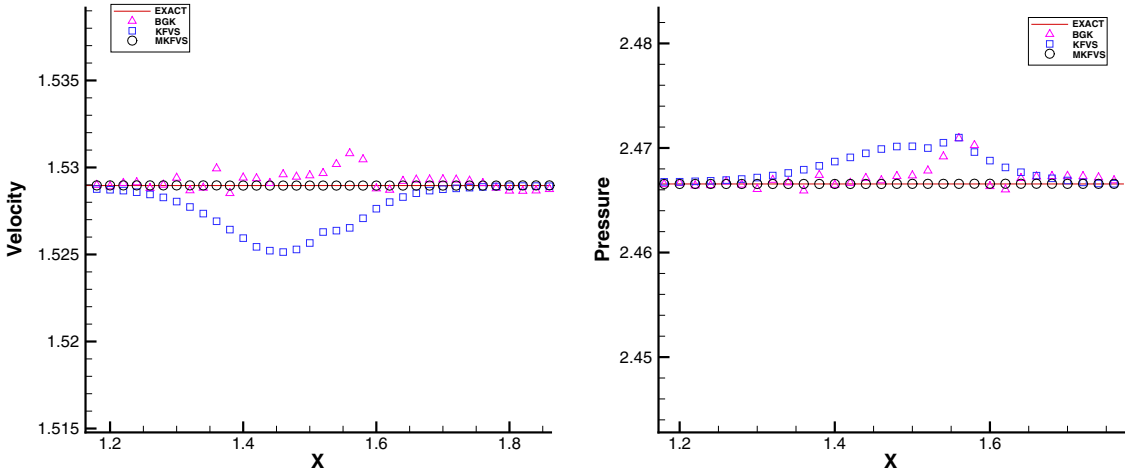

Fig. 6(b). Example 5.3: Close-up in the vicinity of the contact discontinuity in Fig. 5(b). Left: Velocity; Right: Pressure.

$$
\begin{aligned}
(\rho E)_j^{n+1} = &\left(\frac{P}{\gamma-1}+\frac{1}{2}\rho U^2\right)_j^n - \lambda\Bigg\{\Bigg[\left(\frac{P}{\gamma-1}+\frac{1}{2}\rho U^2\right)_j^n \langle u^1\rangle_{j,+} + \frac{1}{2}P_j^n\langle u^1\rangle_{j,+} + \frac{1}{2}P_j^n U_j^n \langle u^0\rangle_{j,+} \\
&+\left(\frac{P}{\gamma-1}+\frac{1}{2}\rho U^2\right)_{j+1}^n \langle u^1\rangle_{j+1,-} + \frac{1}{2}P_{j+1}^n\langle u^1\rangle_{j+1,-} + \frac{1}{2}P_{j+1}^n U_{j+1}^n \langle u^0\rangle_{j+1,-}\Bigg] \\
&-\Bigg[\left(\frac{P}{\gamma-1}+\frac{1}{2}\rho U^2\right)_{j-1}^n \langle u^1\rangle_{j-1,+} + \frac{1}{2}P_{j-1}^n\langle u^1\rangle_{j-1,+} + \frac{1}{2}P_{j-1}^n U_{j-1}^n \langle u^0\rangle_{j-1,+} \\
&+\left(\frac{P}{\gamma-1}+\frac{1}{2}\rho U^2\right)_j^n \langle u^1\rangle_{j,-} + \frac{1}{2}P_j^n\langle u^1\rangle_{j,-} + \frac{1}{2}P_j^n U_j^n \langle u^0\rangle_{j,-}\Bigg]\Bigg\} =: Q_1 + Q_2,
\end{aligned} \tag{4.4}
$$

where

$$
\begin{aligned}
Q_1 &= \left\{\left(\frac{P}{\gamma-1}\right)_j^n - \lambda\left[\left(\left(\frac{P}{\gamma-1}\right)_j^n\langle u^1\rangle_{j,+} + \left(\frac{P}{\gamma-1}\right)_{j+1}^n\langle u^1\rangle_{j+1,-}\right) - \left(\left(\frac{P}{\gamma-1}\right)_{j-1}^n\langle u^1\rangle_{j-1,+} + \left(\frac{P}{\gamma-1}\right)_j^n\langle u^1\rangle_{j,-}\right)\right]\right\} \\
&= P_0\left\{\left(\frac{1}{\gamma-1}\right)_j^n - \lambda\left[\left(\left(\frac{1}{\gamma-1}\right)_j^n\langle u^1\rangle_{j,+} + \left(\frac{1}{(\gamma-1)}\right)_{j+1}^n\langle u^1\rangle_{j+1,-}\right) - \left(\left(\frac{1}{(\gamma-1)}\right)_{j-1}^n\langle u^1\rangle_{j-1,+} + \left(\frac{1}{\gamma-1}\right)_j^n\langle u^1\rangle_{j,-}\right)\right]\right\}
\end{aligned}
$$

and

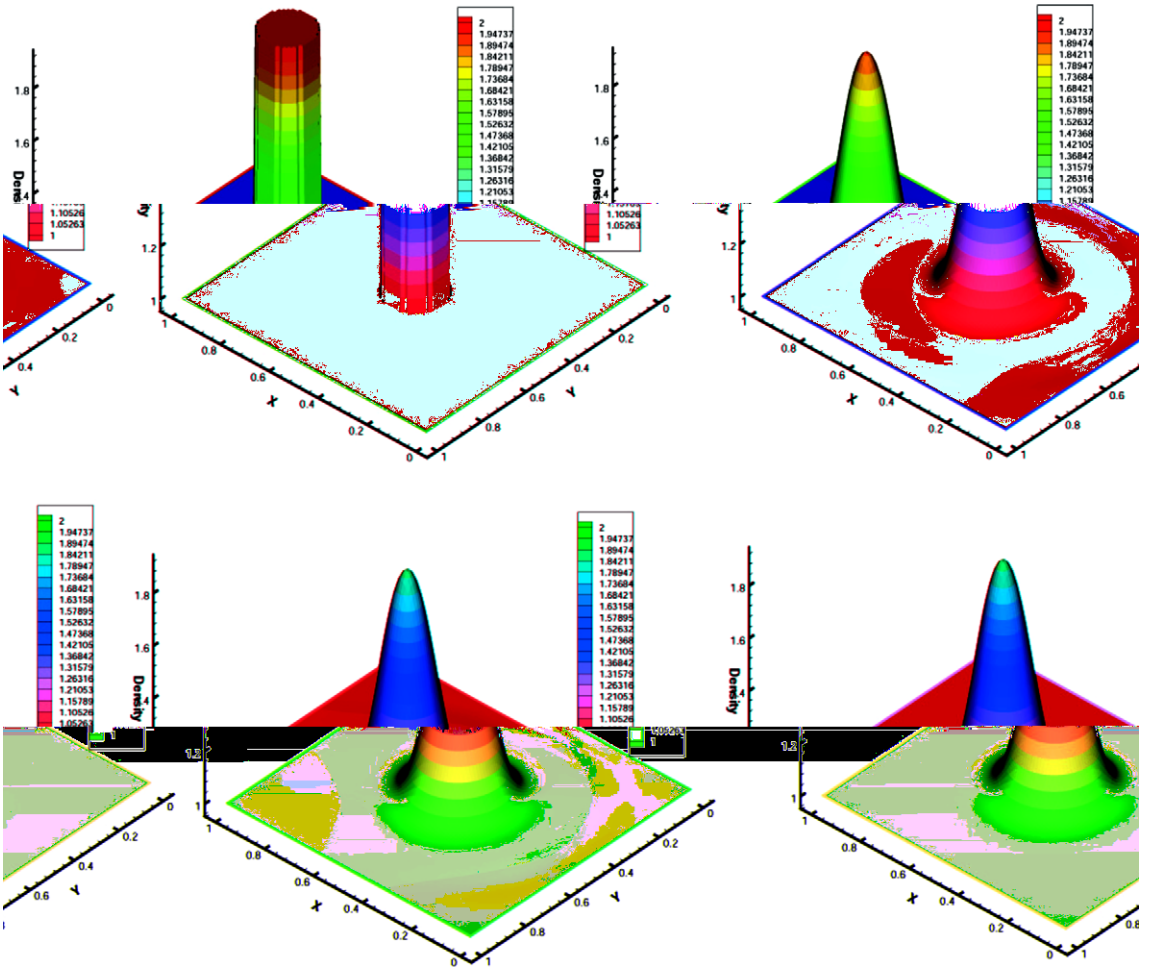

Fig. 7(1a). Example 5.4: Surface plots of the density. Top left: Exact solution; Top right: first-order BGK scheme; Bottom left: first-order KFVS scheme; Bottom right: first-order MKFVS scheme.

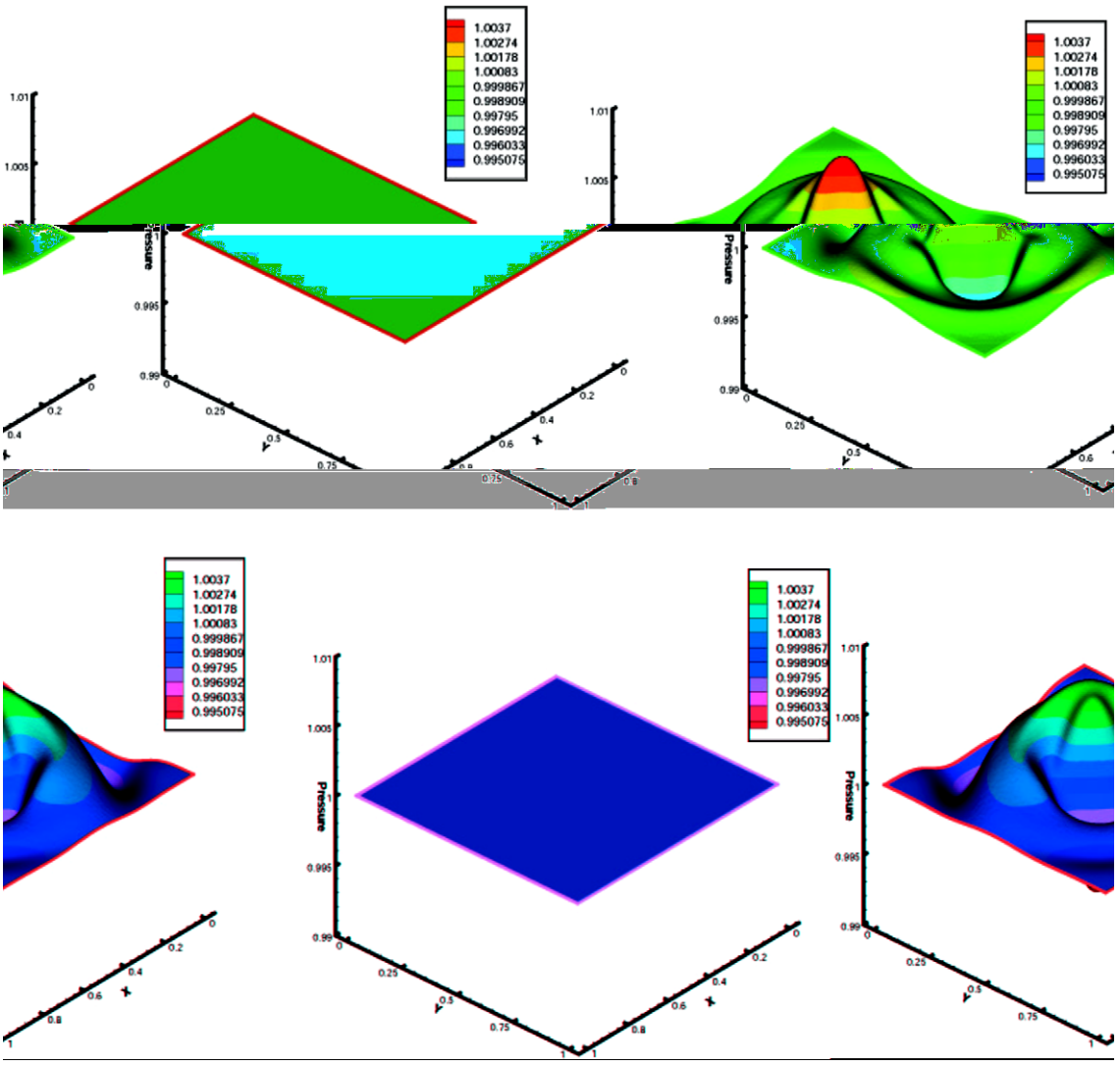

Fig. 7(1b). Example 5.4: Surface plots of the pressure. Top left: Exact solution; Top right: first-order BGK scheme; Bottom left: first-order KFVS scheme; Bottom right: first-order MKFVS scheme.

$$
\begin{aligned}
Q_2 &= \frac{1}{2}(\rho U^2)_j^n - \lambda\Big\{\Big[\frac{1}{2}(\rho U^2)_j^n\langle u^1\rangle_{j,+} + \frac{1}{2}P_j^n\langle u^1\rangle_{j,+} + \frac{1}{2}P_j^n U_j^n\langle u^0\rangle_{j,+} + \frac{1}{2}(\rho U^2)_{j+1}^n\langle u^1\rangle_{j+1,-} + \frac{1}{2}P_{j+1}^n\langle u^1\rangle_{j+1,-} + \frac{1}{2}P_{j+1}^n U_{j+1}^n\langle u^0\rangle_{j+1,-}\Big] \\
&\quad - \Big[\frac{1}{2}(\rho U^2)_{j-1}^n\langle u^1\rangle_{j-1,+} + \frac{1}{2}P_{j-1}^n\langle u^1\rangle_{j-1,+} + \frac{1}{2}P_{j-1}^n U_{j-1}^n\langle u^0\rangle_{j-1,+} + \frac{1}{2}(\rho U^2)_j^n\langle u^1\rangle_{j,-} + \frac{1}{2}P_j^n\langle u^1\rangle_{j,-} + \frac{1}{2}P_j^n U_j^n\langle u^0\rangle_{j,-}\Big]\Big\} \\
&= \frac{1}{2}U_0^2\Big\{\rho_j^n - \lambda\Big[\rho_{j+1}^n\langle u^1\rangle_{j+1,-} + \rho_j^n\langle u^1\rangle_{j,+} - \rho_j^n\langle u^1\rangle_{j,-} - \rho_{j-1}^n\langle u^1\rangle_{j-1,+}\Big]\Big\} - \frac{\lambda}{2}P_0\Big[\langle u^1\rangle_{j+1,-} + \langle u^1\rangle_{j,+} - \langle u^1\rangle_{j,-} - \langle u^1\rangle_{j-1,+}\Big] \\
&\quad - \frac{\lambda}{2}P_0U_0\Big[\langle u^0\rangle_{j+1,-} + \langle u^0\rangle_{j,+} - \langle u^0\rangle_{j,-} - \langle u^0\rangle_{j-1,+}\Big] \\
&= \frac{1}{2}U_0^2\rho_j^{n+1} - \frac{\lambda}{2}P_0U_0\varepsilon_0 - \frac{\lambda}{2}P_0\varepsilon_1
\end{aligned}
$$

with

$$
\begin{aligned}
\varepsilon_1 &= \langle u^1\rangle_{j+1,-} + \langle u^1\rangle_{j,+} - \langle u^1\rangle_{j,-} - \langle u^1\rangle_{j-1,+} \quad \text{and} \\
\varepsilon_0 &= \langle u^0\rangle_{j+1,-} + \langle u^0\rangle_{j,+} - \langle u^0\rangle_{j,-} - \langle u^0\rangle_{j-1,+}.
\end{aligned}
$$

For the MKFVS scheme of first order, one has

$$\varepsilon_1 = \varepsilon_0 = 0, \tag{4.5}$$

which implies $P_j^{n+1} = P_0$. Hence, the discretization of Eq. (4.2) using the first-order MKFVS scheme becomes

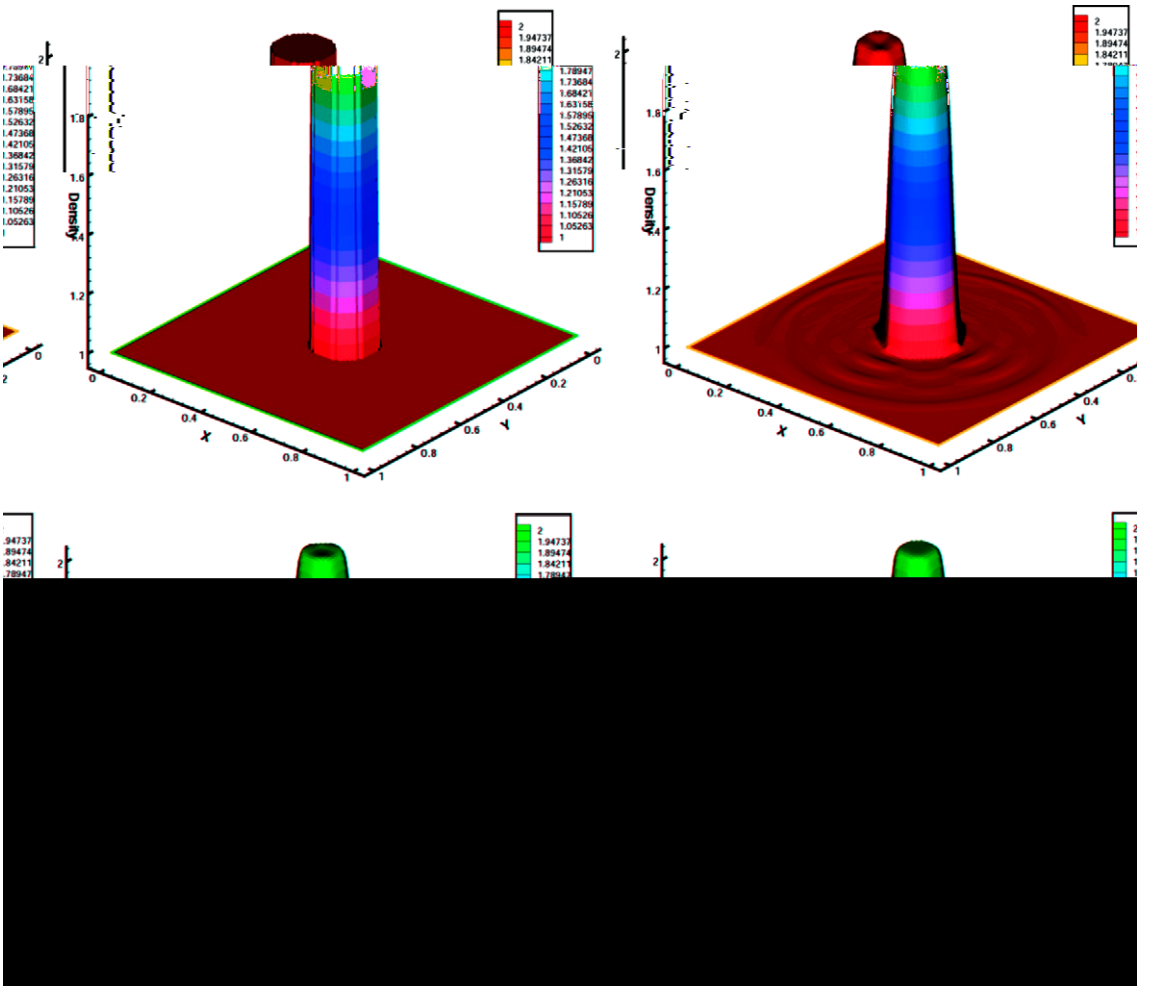

Fig. 7(1c). Example 5.4: Surface plots of the density. Top left: Exact solution; Top right: second-order BGK scheme; Bottom left: first-order KFVS scheme; Bottom right: first-order MKFVS scheme.

$$\left(\frac{1}{\gamma-1}\right)_j^{n+1} = \left(\frac{1}{\gamma-1}\right)_j^{n} - \lambda\left\{\left[\left(\frac{1}{\gamma-1}\right)_j^{n}\langle u^1\rangle_{j,+} + \left(\frac{1}{\gamma-1}\right)_{j+1}^{n}\langle u^1\rangle_{j+1,-}\right] - \left[\left(\frac{1}{\gamma-1}\right)_{j-1}^{n}\langle u^1\rangle_{j-1,+} + \left(\frac{1}{\gamma-1}\right)_j^{n}\langle u^1\rangle_{j,-}\right]\right\}. \tag{4.6}$$

The formula (4.6) can be considered as a discretization of the equation

$$\left[\frac{1}{\gamma-1}\right]_t + \left[\frac{U}{\gamma-1}\right]_x = 0,$$

but not the interface capturing equation (4.2). This means that the disrectization (4.6) cannot give the correct approximate solution of (4.2). To remedy this fault, we rewrite (4.2) as follows:

$$0 = \left[\frac{1}{\gamma-1}\right]_t + U\left[\frac{1}{\gamma-1}\right]_x = \left[\frac{1}{\gamma-1}\right]_t + \left[\frac{U}{\gamma-1}\right]_x - \frac{1}{\gamma-1}U_x, \tag{4.7}$$

and discretize (4.7), instead of using (4.6), as follows:

$$\begin{aligned}\left(\frac{1}{\gamma-1}\right)_j^{n+1} = \left(\frac{1}{\gamma-1}\right)_j^{n} - \lambda\Bigg\{&\left[\left(\left(\frac{1}{\gamma-1}\right)_j^{n}\langle u^1\rangle_{j,+} + \left(\frac{1}{\gamma-1}\right)_{j+1}^{n}\langle u^1\rangle_{j+1,-}\right) - \left(\left(\frac{1}{\gamma-1}\right)_{j-1}^{n}\langle u^1\rangle_{j-1,+} + \left(\frac{1}{\gamma-1}\right)_j^{n}\langle u^1\rangle_{j,-}\right)\right]\\ &+\left(\frac{1}{\gamma-1}\right)_j^{n}\left[\left(\langle u^1\rangle_{j,+} + \langle u^1\rangle_{j+1,-}\right) - \left(\langle u^1\rangle_{j-1,+} + \langle u^1\rangle_{j,-}\right)\right]\Bigg\},\end{aligned} \tag{4.8}$$

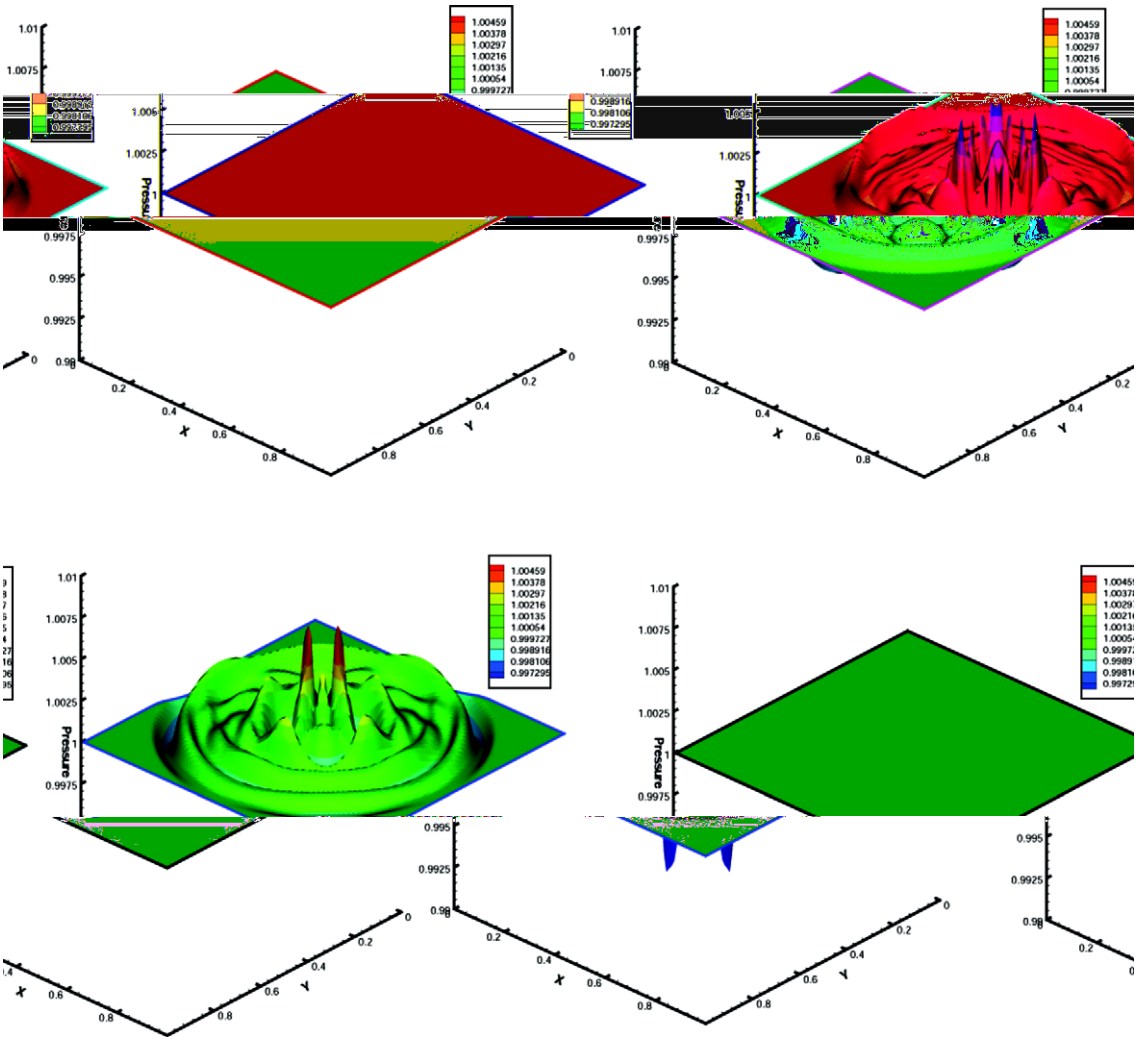

Fig. 7(1d). Example 5.4: Surface plots of the pressure. Top left: Exact solution; Top right: second-order BGK scheme; Bottom left: second-order KFVS scheme; Bottom right: second-order MKFVS scheme.

which is in fact identical to (4.6) in the case that the solution of (2.1), (2.2) and (4.2) consists of only one fluid interface. Therefore, we have proposed a discrete scheme (4.8) for Eq. (4.2) and the scheme is consistent with (4.5). Consequently, the ratio of specific heats γ obtained by solving (4.8) should be oscillation-free across the fluid interface.

Finally, a second-order scheme for multi-fluids can be constructed in a similar way (cf. Section 3), although the calculations involved are more tedious.

5. Numerical experiments

In this section we will compare the KFVS scheme, the BGK scheme and the MKFVS scheme in the following tests. In Examples 5.1–5.4 and we will compare three schemes the KFVS, BGK and MKFVS schemes for single fluids. We take $\eta = 0.7$ for the first-order BGK scheme, while all the parameters in the second-order BGK scheme are from ([20, Chapter 4.2]). In Examples 5.5 and 5.6 we test the current schemes for multi-fluid computations. For the sake of simplicity, we only compare the first- and second-order KFVS and MKFVS schemes, more numerical examples will be tested in the future.

Example 5.1. The first test is an interface only problem with initial data:

$$(\rho, U, P) = \begin{cases} (1, 2, 1) & \text{for } x > 0, \\ (0.1, 2, 1) & \text{for } x < 0. \end{cases}$$

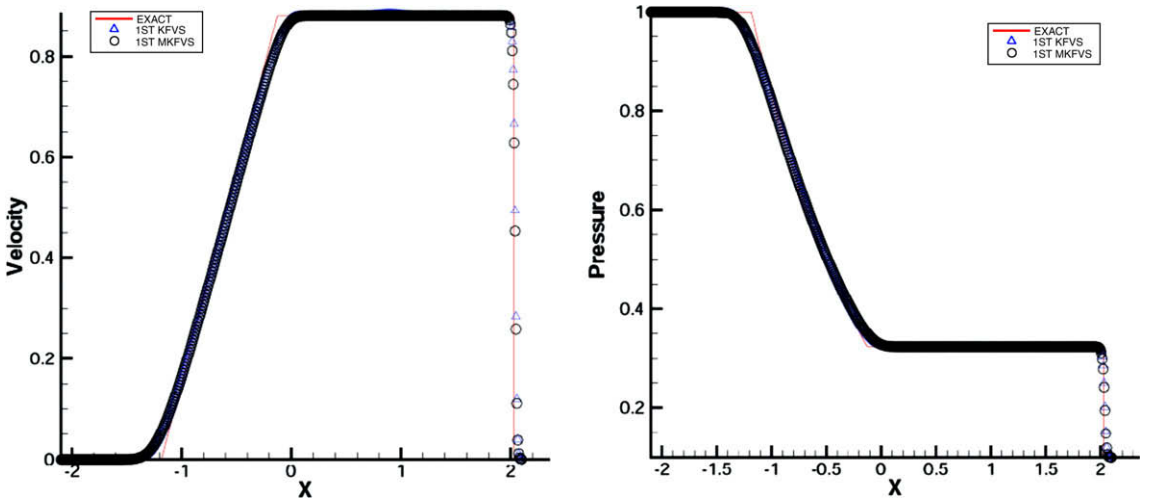

Fig. 8(a). Example 5.5: Computed results at $t = 1.0$ by the first-order KFVS and MKFVS schemes with 500 uniform cells. Left: Velocity; Right: Pressure.

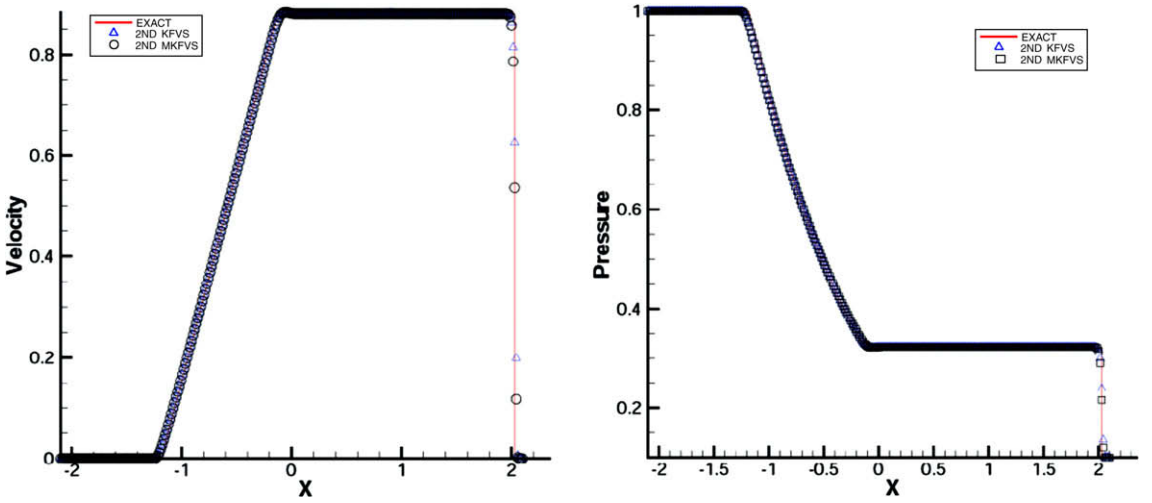

Fig. 8(b). Example 5.5: Computed results at $t = 1.0$ by the second-order KFVS and MKFVS schemes with 300 uniform cells. Left: Velocity; Right: Pressure.

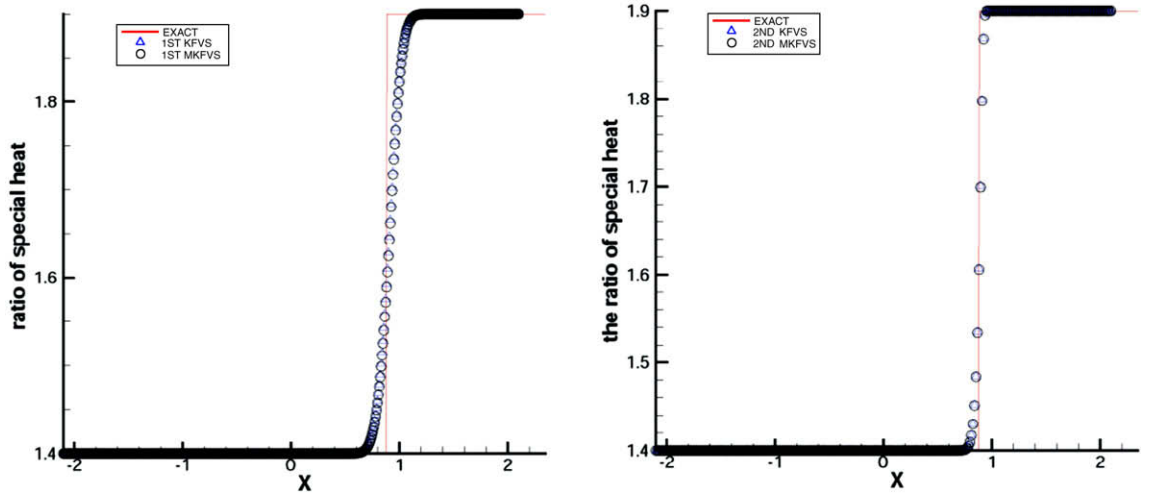

Fig. 8(c). Example 5.5: Computed γ by the KFVS and MKFVS schemes. Left: first-order schemes; Right: second-order schemes.

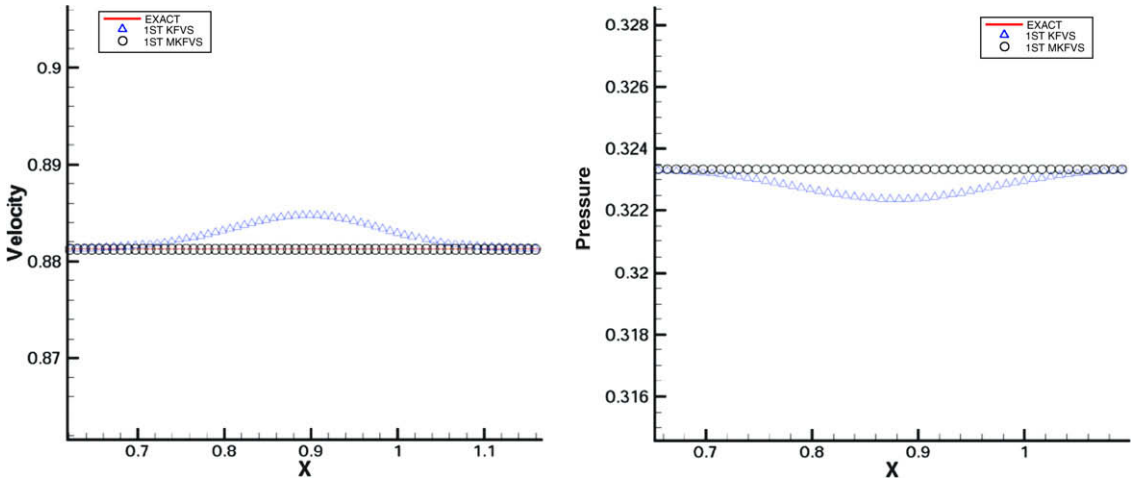

Fig. 9(a). Example 5.5: Close-up of the velocity and the pressure in the vicinity of the contact discontinuity in Fig. 8(a). Left: Velocity; Right: Pressure

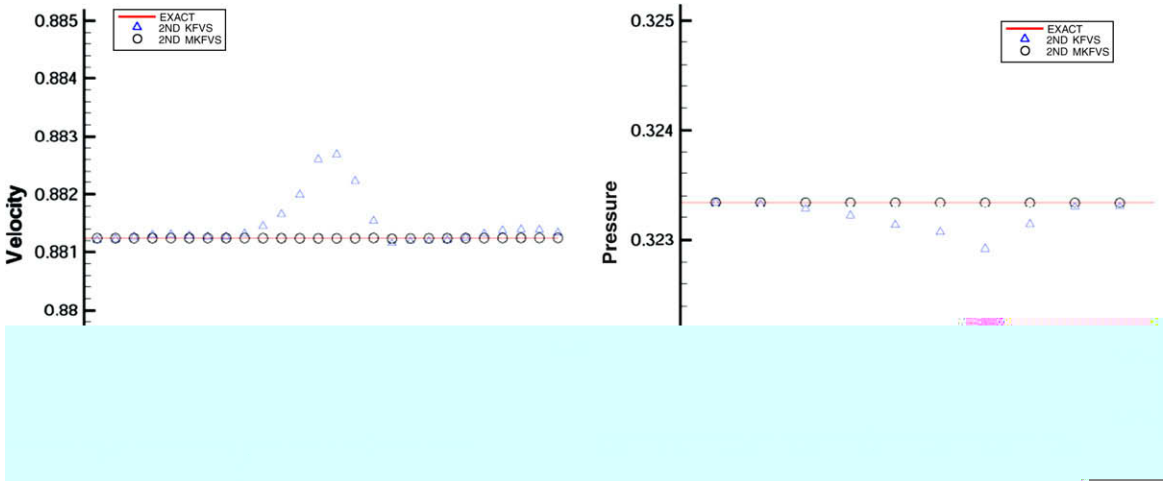

Fig. 9(b). Example 5.5: Close-up of the velocity and the pressure in the vicinity of the contact discontinuity in Fig. 8(b). Left: Velocity; Right: Pressure.

The exact solution for this problem is constant velocity and the pressure. Fig. 1(a) shows the simulation results of the velocity and the pressure using three first-order schemes at one time step with 10 uniform cells, and Fig. 1(b) shows the results of three second-order schemes. It is obvious to see that the BGK and KFVS schemes produce oscillations near the contact discontinuity, although the second-order schemes get better resolution than the first-order schemes, the oscillations do not vanish. At the same time, the first- and second-order MKFVS scheme do not produce any oscillation. Figs. 2(a) and 2(b) give the numerical results with 100 cells at $t = 0.3$. We clearly observe that as the grid is refined, the accuracy is getting improved, the oscillations will not vanish, although they become smaller. On the other hand, the MKFVS schemes have no oscillation across the contact discontinuity. We should point out here that if the parameter such η in the first-order case is appropriately chosen, the oscillation induced by the BGK schemes could diminish. But, how to choose an appropriate parameter is problem- and user's experience-dependent.

Example 5.2 (*Sod's shock problem [18]*). In this calculation, the length of the numerical domain is equal to 6, and 500 cells are used for the first-order scheme while 300 cells are used for the second-order scheme. The initial data are

$$(\rho, U, E) = \begin{cases} (1, 0, 1) & \text{for } x > 0, \\ (0.125, 0, 2) & \text{for } x < 0. \end{cases}$$

The simulation results are given in Figs. 3(a) and 3(b) for the velocity and the pressure at $t = 1.0$ where the solid line is the exact solution. Here we see that all the three schemes perform well. However, if we look at the close-up of the numerical results in the vicinity of the contact discontinuity in Figs. 4(a) and 4(b), we observe that the BGK and KFVS schemes still

produce some oscillations near the contact discontinuity, while no oscillation is found for the MKFVS scheme. Although the oscillations of the BGK and KFVS scheme diminish when the accuracy is improved, they will not vanish. And it is obvious that the BGK scheme is less oscillatory than the KFVS scheme. As mentioned before, we numerically find that the oscillation in the BGK scheme could be diminished, if the parameter η is very carefully chosen.

Example 5.3 (*Lax's shock problem [7]*). In this test the length of the numerical domain is equal to 6, and 500 uniform cells are used for the first-order schemes while 300 cells are used for the second-order schemes. The initial data are

$$(\rho, U, P) = \begin{cases} (0.445, 0.6989, 3.5277) & \text{for } x < 0, \\ (0.5, 0, 0.571) & \text{for } x > 0. \end{cases}$$

Figs. 5(a) and 5(b) show the contours of the velocity and the pressure at $t = 1.0$ of three schemes, and the solid line is the exact solution, while Figs. 6(a) and 6(b) give the close-up of the velocity and the pressure in the vicinity of the contact discontinuity. From Figs. 5 and 6, we draw the same conclusion as in Example 5.2.

Example 5.4 (*2D interface only problem*). Here, we design a two-dimensional interface only problems to compare the three schemes with 100×100 uniform cells. The initial distribution is given by

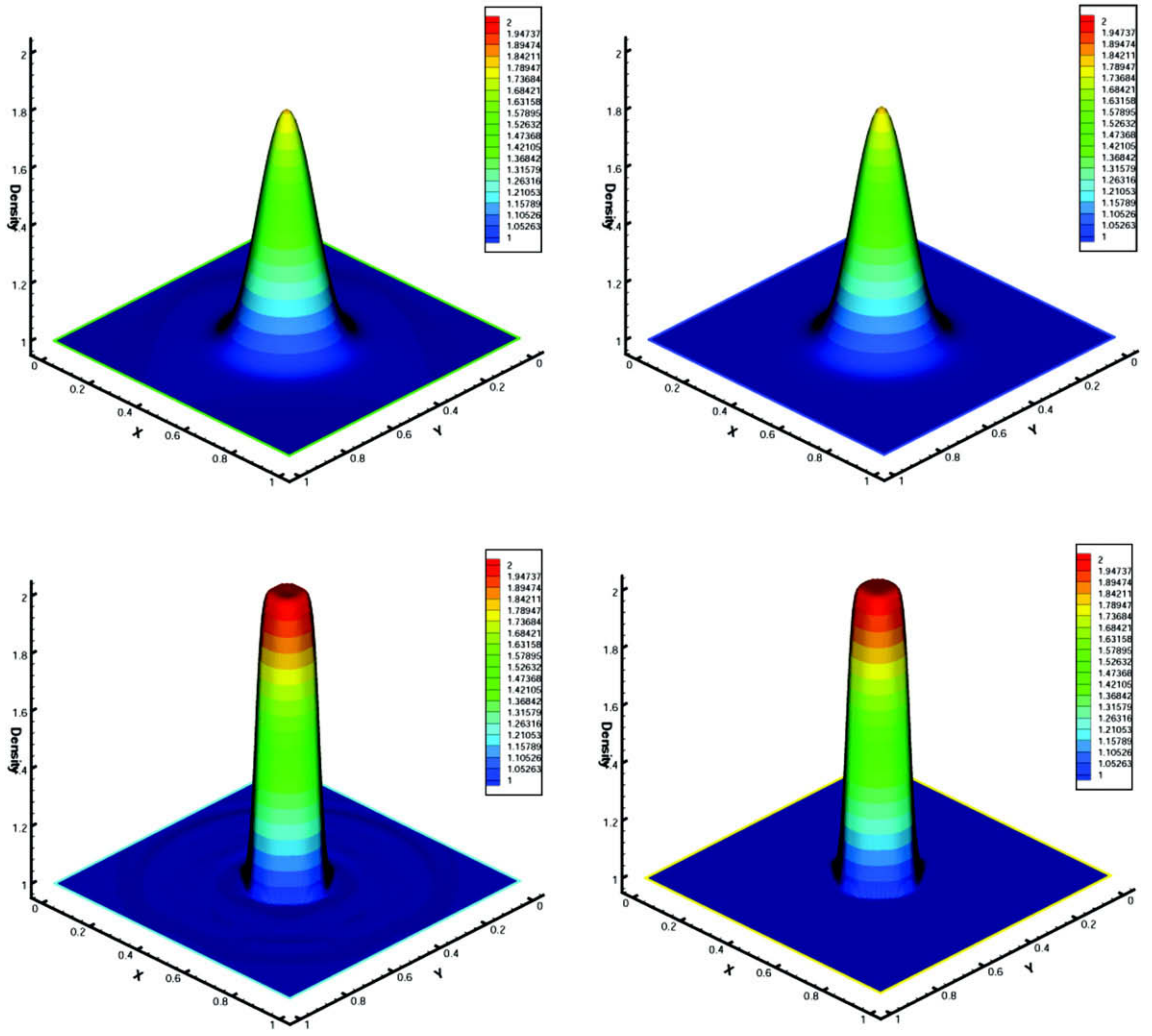

Fig. 10(a). Example 5.6: Surface plots of the density. Top left: first-order KFVS scheme; Top right: first-order MKFVS scheme; Bottom left: second-order KFVS scheme; Bottom right: second-order MKFVS scheme.

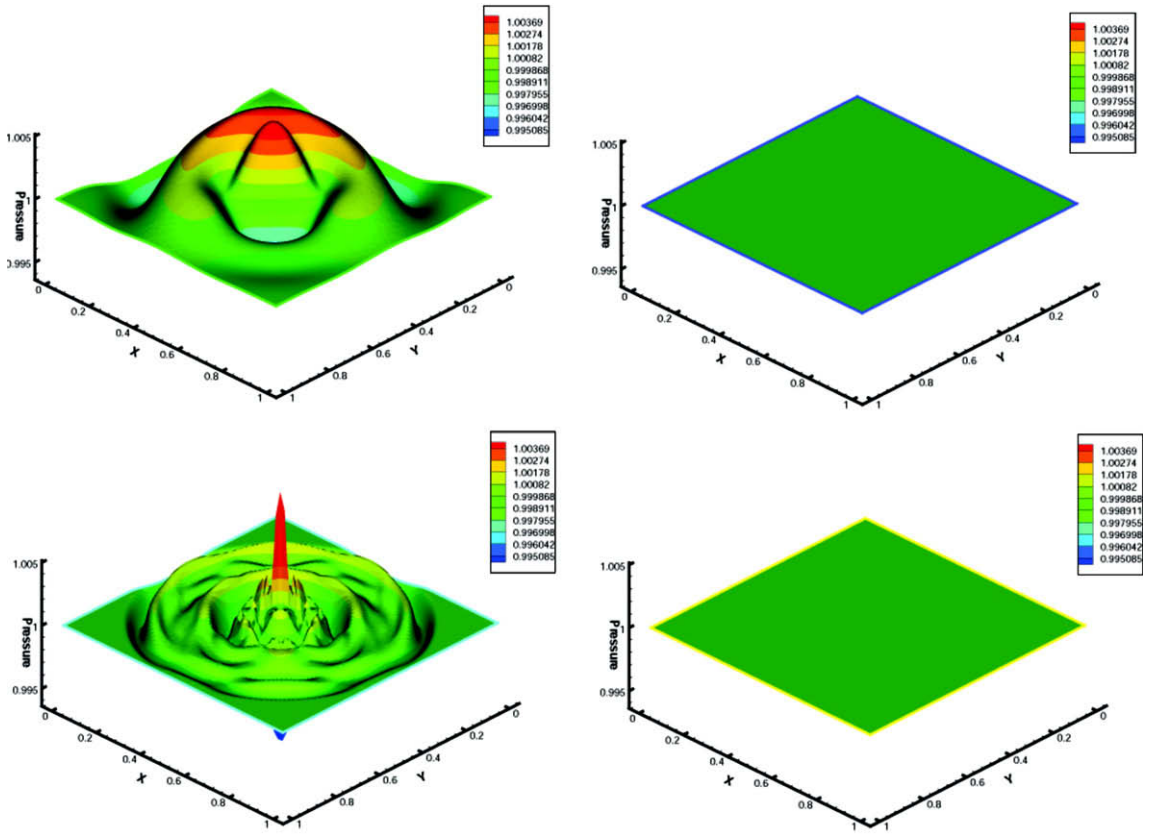

Fig. 10(b). Example 5.6: Surface plots of the pressure. Top left: first-order KFVS scheme; Top right: first-order MKFVS scheme; Bottom left: second-order KFVS scheme; Bottom right: second-order MKFVS scheme.

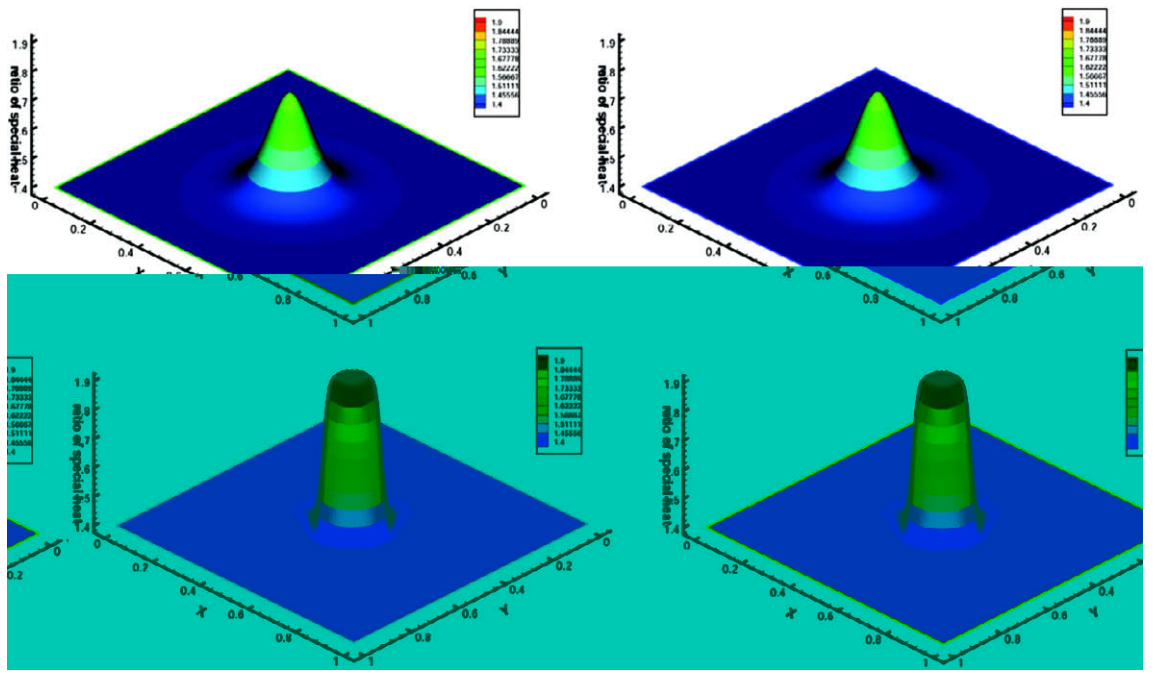

Fig. 10(c). Example 5.6: Surface plots of γ. Top left: first-order KFVS scheme; Top right: first-order MKFVS scheme; Bottom left: second-order KFVS scheme; Bottom right: second-order MKFVS scheme.

$$(\rho, u, v, P) = \begin{cases} (2,1,1,1), \sqrt{((x-0.2)^2+(y-0.2)^2)} < 0.1, \\ (1,1,1,1), \sqrt{((x-0.2)^2+(y-0.2)^2)} > 0.1 \end{cases}$$

and the corresponding exact solution at $t = 0.3$ is given by

$$(\rho, u, v, P) = \begin{cases} (2,1,1,1), \sqrt{((x-0.5)^2+(y-0.5)^2)} < 0.1, \\ (1,1,1,1), \sqrt{((x-0.5)^2+(y-0.5)^2)} > 0.1. \end{cases}$$

Figs. 7(1a) and 7(1c) show the computed results using the first-order schemes, while Figs. 7(1b) and 7(1d) give the computed results using the second-order schemes. In Figs. 7(1a) and 7(1b) the density distribution is shown, and it is obvious that the second-order schemes resolve sharper than the first-order ones. The pressure distribution is given in Figs. 7(1c) and 7(1d), from which we find that the BGK and KFVS schemes produce oscillations that will not vanish as the accuracy is improved. On the other hand, the first- and second-order MKFVS schemes keep a good resolution for the velocity and pressure.

In the following two examples, we test our MFKVS schemes for multi-fluid computations.

Example 5.5 (*1D multi-fluid problem*). In this example, we use the MKFVS scheme constructed in Section 4 to simulate a 1D multi-fluid problem. Since our MKFVS is modified from the KFVS scheme, we compare the MKFVS scheme with the KFVS scheme. In this calculation, the length of the numerical domain is equal to 6, and 500 cells are used for the first-order scheme while 300 cells are used for the second-order scheme. The initial data read

$$(\rho, U, P, \gamma) = \begin{cases} (1,0,1,1.4) & \text{for } x > 0, \\ (0.125,0,0.1,1.9) & \text{for } x < 0. \end{cases}$$

In Fig. 8(a) the velocity and pressure computed by the first-order KFVS and MKFVS schemes are shown, while in Fig. 8(b) the numerical results using the second-order schemes are given, and in Fig. 8(c) the results of γ using all the four schemes are presented. Figs. 9(a) and 9(b) show the close-up of the numerical results in the vicinity of the contact discontinuity. In general, both schemes performs well. However, comparing with the exact solution, the second-order schemes perform clearly better than the first-order ones, the KFVS schemes produce small oscillations near the fluid interface, while the MKFVS give the exact solution. This demonstrates that the second-order MKFVS scheme also works well for multi-fluid problems.

Example 5.6 (*2D interface only problem*). Here, we extend a two-dimensional interface only problems to a multi-fluid to compare the MKFVS and KFVS schemes. The initial distribution is given by

$$(\rho, u, v, P, \gamma) = \begin{cases} (2,1,1,1,1.4), \sqrt{((x-0.2)^2+(y-0.2)^2)} < 0.1, \\ (1,1,1,1,1.9), \sqrt{((x-0.2)^2+(y-0.2)^2)} > 0.1 \end{cases}$$

and the corresponding exact solution at $t = 0.3$ is

$$(\rho, u, v, P, \gamma) = \begin{cases} (2,1,1,1,1.4), \sqrt{((x-0.5)^2+(y-0.5)^2)} < 0.1, \\ (1,1,1,1,1.9), \sqrt{((x-0.5)^2+(y-0.5)^2)} > 0.1. \end{cases}$$

The computation domain is $[0,1] \times [0,1]$, a 100×100 uniform grid is used.

Figs. 10(a), 10(b), 10(c) are the numerical results computed by the first- and second-order KFVS and MKFVS schemes. In general, both schemes work well for this multi-fluid problem. But, from Figs. 10(a) and 10(c) where the density and γ distributions are given, it is obvious to observe that the second-order schemes resolve the fluid interface apparently sharper than the first-order ones. Fig. 10(b) is the pressure distribution, we find that both the first- and second-order KFVS schemes produce small oscillations near the fluid interface and the oscillations will not vanish as the accuracy is improved, while there is no oscillation for the first- and second-order MKFVS schemes. This also shows that our second-order MKFVS scheme performs well for multi-fluid problems.

6. Conclusion

In this paper, based on a careful study of the behavior of the discrete physical variables across the contact discontinuity, we have analyzed quantitatively the mechanism of inducing spurious oscillations of the velocity and the pressure in the vicinity of the contact discontinuity for the first-order kinetic flux vector splitting (KFVS) and BGK schemes for compressible flows, and found that if certain consistent conditions hold, then the spurious oscillations vanish. Then, with the help of this analysis, we have proposed a first-order modified KFVS (MKFVS) scheme which is oscillation-free in the vicinity of the con-

tact discontinuity. Furthermore, by employing piecewise linear reconstruction of the initial data and van Leer's limiter, the first-order MKFVS scheme is extended to a second-order one, and consequently, we have constructed a nonoscillatory second-order MKFVS scheme. Finally, by combing the MKFVS schemes with the γ-model, we have successfully extended the MKFVS schemes to multi-flows and proposed therefore a first- and second-order MKFVS schemes for multi-fluid simulations, which are also nonoscillatory across fluid interfaces. We have carried out a number of tests inclusive of multi-fluid problems. The numerical results validate the theoretic analysis and demonstrate the good performance of the MKFVS schemes in the simulation of contact discontinuities for both single- and multi-fluids. Moreover, the second-order MKFVS scheme resolves shock waves clearly better than the first-order one. This demonstrates that after an appropriate modification of the original first- and second-order KFVS schemes, the modified schemes become more credible and robust.

Acknowledgments

The authors would like to thank Professor Kun Xu and Zhong Lin for the constructive discussions. Part of this work was done when Chen was visiting University of Science and Technology, Hong Kong. He wishes to thank Professor Kun Xu for his kind hospitality.

References

[1] R. Abgrall, How to prevent pressure oscillations in multicomponent flow calculation: a quasi conservative approach, J. Comput. Phys. 125 (1996) 150–160.
[2] R. Abgrall, S. Karni, Computations of compressible multifluids, J. Comput. Phys. 169 (2001) 594–623.
[3] S.Y. Chou, D. Baganoff, Kinetic flux vector splitting for the Navier–Stokes equations, J. Comput. Phys. 130 (1997) 217–230.
[4] S.M. Deshpande, A second order accurate, kinetic-theory based, method for inviscid compressible flows, NASA Langley Tech. Paper No. 2613, 1986.
[5] T.G. Elizarova, B.N. Chetverushkin, Kinetic algorithms for calculating gas dynamic flows, J. Comput. Math. Math. Phys. 25 (1985) 1526–1533.
[6] X.Y. He, L.S. Luo, Theory of the lattice Boltzmann method: from the Boltzmann equation to the lattice Boltzmann equation, Phys. Rev. E 56 (1997) 6811–6817.
[7] P.D. Lax, Weak solutions of nonlinear hyperbolic equations and their numerical computation, Commun. Pure Appl. Math. 7 (1954) 159–193.
[8] M.N. Macrossan, R.I. Oliver, A kinetic theory solution method for the Navier–Stokes equations, Int. J. Numer. Meth. Fluids 17 (1993) 177–193.
[9] J.C. Mandal, S.M. Deshpande, Kinetic flux vector splitting for the Euler equations, Comp. Fluids 23 (1994) 447–478.
[10] G. May, A. Jameson, Unstructured algorithm for the inviscid and viscous flows embedded in a unified solver architecture: Flo3xx. AIAA Paper, 2005-0318, 2005.
[11] G. May, B. Srinivasan, A. Jameson, An improved gas-kinetic BGK finite volume method for three-dimensional transonic flow, J. Comput. Phys. 220 (2007) 856–878.
[12] J.M. Moschetta, D. Pullin, A robust low diffusive kinetic scheme for the Navier–Stokes/Euler equations, J. Comput. Phys. 133 (1997) 193–204.
[13] T. Ohwada, On the construction of kinetic scheme, J. Comput. Phys. 177 (2002) 156–175.
[14] B. Perthame, Second-order Boltzmann schemes for compressible Euler equation in one and two space dimensions, SIAM J. Numer. Anal. 29 (1992) 1–19.
[15] K.H. Prendergast, K. Xu, Numerical hydrodynamics from gas kinetic theory, J. Comput. Phys. 109 (1993) 53–66.
[16] D.I. Pullin, Direct simulation methods for compressible inviscid ideal gas flow, J. Comput. Phys. 34 (1980) 231–244.
[17] R.D. Reitz, One-dimensional compressible gas dynamics calculations using the Boltzmann equations, J. Comput. Phys. 42 (1981) 108–123.
[18] G.A. Sod, Review a survey of several finite difference method of system of nonlinear hyperbolic conservation laws, J. Comput. Phys. 27 (1978) 1–31.
[19] K. Xu, Numerical Hydrodynamics From Gas-Kinetic Theory, Ph.D. Thesis, Columbia University, USA, 1993.
[20] K. Xu, Gas-Kinetic Schemes for Unsteady Compressible Flow Simulations, von Karman Institute for Fluid Dynamics Lecture Series, 1998–03, 1998.
[21] K. Xu, A gas-kinetic BGK scheme for the Navier–Stokes equations and its connection with artificial dissipation and Godunov method, J. Comput. Phys. 171 (2001) 289–335.
[22] K. Xu, K.H. Prendergast, Numerical Navier–Stokes solutions from gas kinetic theory, J. Comput. Phys. 114 (1994) 9–17.